Pressurized Gas eXpanded (PGX) liquid drying of sodium alginate and its loading with coenzyme Q10 by adsorptive precipitation

by

Zixiang Liu

A thesis submitted in partial fulfillment of the requirements for the degree of

Master of Science

in

Food Science and Technology

Department of Agricultural, Food and Nutritional Science
University of Alberta

Abstract

Pressurized Gas eXpanded (PGX) liquid technology is a particle formation technique based on the use of carbon dioxide (CO_2) and ethanol as the drying fluid. This technology uses an anti-solvent method to precipitate water-soluble biopolymers from aqueous solution and produces micro- or nano-sized particles with unique morphology. Adsorptive precipitation is a method for preparing delivery systems based on the application of supercritical carbon dioxide (SC-CO_2), where a hydrophobic bioactive compound can be loaded on a polymer carrier without the use of any organic solvent during the process. In this thesis research, PGX processing of sodium alginate (SA), and its loading with coenzyme Q10 (CoQ10), a potent antioxidant, by adsorptive precipitation were investigated, in terms of the impact of processing parameters on their physicochemical properties.

For the PGX-processed sodium alginate (PGX-SA), different characterizations such as surface area, morphology, thermal behavior, and viscosity were performed for better understanding of the effect of different processing parameters. PGX-SA had a fibrous structure with a fine network of fibrils, compared to the fine particles with a smooth surface of the unprocessed SA. In addition to the change in the morphology of the particles, the surface area was increased and the bulk density was decreased by more than 120 times compared to the unprocessed SA. Use of low concentration (1.0% w/w) of the SA aqueous solution as the feed material, low ethanol flow rate (15 g/min), with the mass flow rate ratio of 4:15:5 of aqueous solution:ethanol:CO_2 resulted in the surface area of 164.5 m^2/g of the PGX-SA. The viscosity of

the PGX-SA solution was similar to that of the unprocessed SA at the same concentration, which indicated that the molecular weight was not affected by the PGX process.

The CoQ10-loaded PGX-SA (L-SA) obtained by adsorptive precipitation under different processing conditions was investigated for its CoQ10 loading content, morphology, thermal behavior, crystallinity of CoQ10, and dispersion stability in the aqueous system. High circulation power (50 min X 262 mL/min), low operation pressure (200 bar), and the biopolymer with a high surface area (ground PGX-SA) resulted in a higher loading. The highest CoQ10 loading obtained in this study was 46.9% w/w. Helium ion microscopy images demonstrated a uniform coating of CoQ10 on the surface of PGX-SA. The loaded CoQ10 was in the crystalline form based on the results from thermal and crystallinity analysis. The aqueous dispersion of L-SA was stable after 50 days of storage in the dark environment at 4 ºC with some CoQ10 precipitation.

The findings provide guidance for further development of the PGX technology, and demonstrate its potential for developing new bioactive delivery systems, especially targeting applications of hydrophobic bioactive compounds such as CoQ10 in aqueous-based products.

Preface

This thesis is an original work by Zixiang Liu under the supervision of Dr. Feral Temelli, comprised of five chapters: Chapter 1 provides background information and thesis research objectives; Chapter 2 is literature review related to the topics of the two studies; Chapter 3 is focused on the drying of sodium alginate (SA) using PGX technology; Chapter 4 is on adsorptive precipitation of CoQ10 on PGX-SA; and Chapter 5 provides overall conclusions and recommendations for future work.

Manuscripts based on Chapters 3 and 4 are in preparation for submission to peer-reviewed journals. Main findings and conclusions from Chapter 3 were presented at the 17th European Meeting on Supercritical Fluids as an oral presentation in Ciudad Real, Spain, April 8-11, 2019. Part of the results from Chapters 3 and 4 were presented at the 16th Annual Natural Health Products Research Conference as a poster presentation in Edmonton, AB, Canada, May 27-29, 2019.

Acknowledgements

I would like to thank my great supervisor Dr. Feral Temelli, without your help, support, patience, and encouragement, it would not have been possible for me to complete my research and thesis. I still remember before I came to Canada, Dr. Ozan Ciftci told me that you are the best, and now I understand why and totally agree with him. Your positive energy and emotion, as well as your great interpersonal skills are always encouraging me to improve myself as much as I can.

Thank you, Dr. Jonathan Curtis, for consistently providing advice and helping me with different kinds of sample analysis, as well as being my supervisory committee member. Also, I am grateful to the help of Dr. Roopesh Mohandas Syamaladevi to be my thesis defence examination committee member and to provide me feedback for this thesis.

Thanks to the Natural Sciences and Engineering Research Council of Canada (NSERC), and Ceapro Inc. for their financial support of my research project.

I am grateful for the help of Dr. Ricardo Tomas Do Couto for giving me support and advice during my two-year-study. Thanks to Ereddad Kharraz and Dr. Tolibjon Omonov from Dr. Jonathan Curtis' lab to help me with my DSC analysis and giving me feedback and advice for my sample characterizations. Also, I would like to thank Dr. Paul Moquin, Dr. Bernhard Seifried, Dr. Byron Yépez, and Emily Wong from Ceapro Inc. for their suggestions during my study and research, as well as providing me PGX-processed sodium alginate samples for my adsorptive precipitation study. Furthermore, I would like to thank my lab family members, Yonas

Gebrehiwot, Dr. David Villanueva Bermejo, Brasathe Jeganathan, Yanzhao Ren, Carla Valdivieso, Eileen Santos, Andrea Carolina Vilchez, Sule Keskin Ulug, and Dr. Karina Araus Sermiento for their support and inspirations.

Last but not least, I would like to thank my family and my friends for their consistent love and support. Life is so good to be together with you.

Table of contents

Chapter 1: Introduction and objectives……...……1

Chapter 2: Literature review……4

2.1 Sodium alginate……..4

2.1.1 Sources and structure……4

2.1.2 Extraction of sodium alginate……...6

2.1.3 Physicochemical properties……..7

2.1.4 Applications in food products……...8

2.2 Coenzyme Q10……..9

2.2.1 Sources and structure……9

2.2.2 Health benefits……...….11

2.3 Polysaccharide drying methods……...…13

2.3.1 Traditional methods……..…….13

2.3.2 Supercritical CO_2-based methods……..……14

2.4 Delivery systems involving sodium alginate and CoQ10……18

2.4.1 Traditional delivery methods for CoQ10……18

2.4.2 Adsorptive precipitation method…….21

Chapter 3: Drying of sodium alginate using Pressurized Gas eXpanded (PGX) liquid technology…….25

3.1 Introduction……...25

3.2 Materials and methods……..……....26

3.2.1 Materials……..…..…26

3.2.2 PGX unit……..…..…27

3.2.3 Experimental design……....29

3.2.4 Characterization of SA particles……..…32

3.2.4.1 Viscosity measurement…….32

3.2.4.2 Particle morphology…….….33

3.2.4.3 Surface area analysis……33
3.2.4.4 Differential scanning calorimetry analysis……...33
3.2.4.5 Fourier-transform infrared spectroscopy analysis……34
3.2.4.6 X-ray diffraction analysis…….34
3.2.4.7 Bulk density measurement……34
3.2.4.8 Statistical analysis…….35
3.3 Results and discussion……..35
3.3.1 Viscosity measurement……...……35
3.3.2 Morphology……36
3.3.3 Surface area……38
3.3.4 Differential scanning calorimetry……...41
3.3.5 Fourier-transform infrared spectroscopy……43
3.3.6 X-ray diffraction analysis……...45
3.3.7 Bulk density……46
3.4 Conclusions……..48

Chapter 4: Adsorptive precipitation of coenzyme Q10 on sodium alginate dried using Pressurized Gas eXpanded liquid technology……..……49
4.1 Introduction……...49
4.2 Materials and methods……..51
4.2.1 Materials…….51
4.2.2 Adsorptive precipitation unit……..51
4.2.3 Experimental design……54
4.2.4 Characterization of loaded products……...…55
4.2.4.1 CoQ10 loading content……..…...55
4.2.4.2 Particle morphology……...56
4.2.4.3 Differential scanning calorimetry analysis……..….57
4.2.4.4 Fourier-transform infrared spectroscopy analysis……..…..57
4.2.4.5 X-ray diffraction analysis……..……...57
4.2.4.6 Dispersion in aqueous system and storage stability test……..57

4.2.4.7 Zeta potential of dispersion in aqueous system……..…..57
4.2.4.8 Statistical analysis…….58
4.3 Results and discussion……..58
4.3.1 CoQ10 loading……58
4.3.2 Morphology…….62
4.3.3 Fourier-transform infrared spectroscopy……...….63
4.3.4 Differential scanning calorimetry……...….66
4.3.5 X-ray diffraction analysis……..…….67
4.3.6 Dispersion in aqueous system……..…..70
4.3.7 Zeta potential……..……....71
4.4 Conclusions……..73

Chapter 5: Conclusions and Recommendations……..…….74
5.1 Summary of key findings……..……....74
5.2 Recommendations for future work……...….77

Bibliography……80

List of Tables

Table 3.1 Experimental conditions tested for PGX drying of SA…….30

Table 4.1 Experimental conditions tested for adsorptive precipitation of CoQ10 on PGX-SA……..……...55

List of Figures

Figure 2.1 Structural characteristics of alginate: G-block (top), M-block (middle), and alternating M and G-block (bottom). Reprinted from Lee and Mooney (2012) with permission from Elsevier……5

Figure 2.2 Chemical structure of CoQ10……..……..9

Figure 2.3 Chemical structure of quinones, semiquinones, and quinols. Reprinted from Song and Buettner (2010) with permission from Elsevier.……10

Figure 2.4 Ternary phase diagram for water-ehtanol-CO_2 mixture at 40 °C. Reprinted from Durling et al. (2007) with permission from Elsevier.……..…..17

Figure 3.1 Flow chart of the PGX unit. CV: check-valve; V: valve; PI: pressure gauge; BPR: back pressure regulator…….....28

Figure 3.2 Ternary diagram of water, EtOH, and CO_2 at 100 bar and 40 °C. Data for plotting this ternary diagram was obtained from Durling et al. (2007) ……32

Figure 3.3 Effect of SA concentration on the viscosity of unprocessed SA and PGX-processed SA aqueous solutions (mass flow rate ratio 4:15:5, 15 g/min ethanol flow rate, 1.0% feed conc.) measured at 20 °C.……36

Figure 3.4 HIM images of unprocessed SA (top row), and PGX-processed SA (bottom row) at mass flow rate ratio of 4:15:5, and 15 g/min ethanol flow rate, and 1.0% w/w SA solution……37

Figure 3.5 HIM images of PGX-processed SA (1.0% w/w). Each row represents different EtOH flow rates, and each column represents different mass flow rate ratios……38

Figure 3.6 PGX-processed SA (mass flow rate ratio 4:15:5, 15 g/min ethanol flow rate) at different aqueous solution concentrations (left 1.5% w/w, right 2.0% w/w) ……38

Figure 3.7 Specific surface area of unprocessed SA, 1.0% (w/w) spray dried SA, and the range for 1.0% (w/w) PGX-dried SA obtained at different conditions…..…….....40

Figure 3.8 Specific surface area of PGX-dried SA (1.0% w/w) obtained at different EtOH flow rates and mass flow rate ratios of SA solution: EtOH: CO_2. Error bars represent mean±standard deviation based on duplicate runs…….40

Figure 3.9 Specific surface area of PGX dried SA (mass flow rate ratio 4:15:5, 15 g/min ethanol flow rate) at different SA concentrations of aqueous polymer solution. Error bars represent

mean±standard deviation based on duplicate runs.……41
Figure 3.10 DSC thermograms of unprocessed, and PGX-processed SA samples……...43
Figure 3.11 FTIR spectra of unprocessed SA, spray dried, and PGX-processed SA……...45
Figure 3.12 XRD analysis of unprocessed (blue color) and PGX-processed (orange color) SA……..46
Figure 3.13 Bulk density of unprocessed, spray dried, and PGX-dried SA……..…...47
Figure 4.1 Flow chart of the adsorptive precipitation unit.……..53
Figure 4.2 CoQ10 loading obtained at different processing conditions. O (original form of the PGX-SA), G (ground form of the PGX-SA).……59
Figure 4.3 HIM images of PGX-SA, L-SA (processed at 300 bar, 40 min & 262 mL/min, original form), and 30% physical mixture of CoQ10 and PGX-SA……..63
Figure 4.4 FTIR spectra for physical mixture and L-SA……..65
Figure 4.5 FTIR spectra for CoQ10 and L-SA…….65
Figure 4.6 DSC analysis results (L-SA-01 was processed at 300 bar, with 40 min & 262 mL/min, and biopolymer in original form; L-SA-02 was processed at the same conditions using biopolymer in ground form) …….67
Figure 4.7 XRD spectra (from top to bottom) of CoQ10, PM, L-SA (processed at 300 bar, with 40 min & 262 mL/min, and biopolymer in original form), and PGX-SA.……...…….69
Figure 4.8 Photographs of aqueous dispersions. (left) aqueous dispersion of PGX-SA, PM, and L-SA; (right) close up of physical mixture…….…….…..70
Figure 4.9 Aqueous dispersions of L-SA after 3 (left) and 50 (right) days storage at 4 ºC.…….71
Figure 4.10 Zeta potential values of different samples (L-SA-01 was processed at 300 bar, with 40 min & 262 mL/min circulation, and biopolymer in original form; L-SA-02 was processed at similar conditions except at 200 bar; and L-SA-03 was processed at similar conditions to L-SA-01 but using biopolymer in ground form).……..72

List of Abbreviations

ADP	Adenosine diphosphate
ANOVA	Analysis of variance
ATP	Adenosine triphosphate
BET	Brunauer–Emmett–Teller
CO_2	Carbon dioxide
CoQ10	Coenzyme Q10
CV	Check valve
DSC	Differential scanning calorimeter
ELAS	Expanded liquid antisolvent process
EtOH	Ethanol
FTIR	Fourier transform infrared spectrophotometry
G	α-L-guluronate
GAS	Gas-antisolvent process
HIM	Helium ion microscopy
L-SA	CoQ10-loaded PGX-SA
M	β-D-mannuronate
MW	Molecular weight
NMR	Nuclear magnetic resonance
PGSS	Particles from gas saturated solutions
PGX	Pressurized gas expanded liquid
PI	Pressure gauge
PM	Physical mixture
PGX-SA	PGX-processed sodium alginate
RESS	Rapid expansion of supercritical solution
SA	Sodium alginate
SAS	Supercritical antisolvent process
SC-CO_2	Supercritical carbon dioxide
UV	Ultraviolet light

V	Valve
XRD	X-Ray diffraction

Chapter 1: Introduction and objectives

Supercritical carbon dioxide (SC-CO_2) is achieved when CO_2 is pressurized and heated up to conditions above its critical point (31.1 °C and 73.8 bar). In the supercritical fluid region, CO_2 exhibits properties of both liquid and gas state CO_2. Due to the unique properties of SC-CO_2, such as high diffusivity, low viscosity, and no surface tension, it has been applied in many studies, targeting extraction of various plant materials and particle formation among others over the decades. Pressurized Gas eXpanded (PGX) liquid technology is a particle formation technique based on the application of CO_2, which was invented by Temelli and Seifried (2016). This technology uses an anti-solvent method to precipitate water-soluble biopolymers from aqueous solution and produces micro- or nano-sized particles with unique morphology that cannot be achieved by any other conventional drying method. Adsorptive precipitation is another application of SC-CO_2, where a hydrophobic bioactive compound can be loaded on a polymer carrier. SC-CO_2 is used to solubilize a hydrophobic compound and serves as the carrying medium to load it onto the biopolymer. This is an environmentally-friendly process, which can result in the bioactive compound being loading homogeneously onto the biopolymer without the use of any organic solvent during the process.

The water-soluble biopolymer used in this research is sodium alginate (SA), which is a polysaccharide extracted from brown algae. The SA is a long-chain, high-molecular-weight polysaccharide, which can solubilize in water to form high viscosity solutions, and form a gel when combined with multivalent cations, like calcium. Therefore, it has been utilized in many

studies related to gel formation and encapsulation of various bioactive compounds. However, the PGX drying of an aqueous solution of SA has not been studied in detail and it is not known what kind of unique properties can be achieved by this technology.

The coenzyme Q10 (CoQ10) was chosen as the bioactive compound to investigate in this research since the adsorptive precipitation of CoQ10 on SA has not been reported previously. CoQ10 is present in the membrane system of all aerobic respiration cells, and plays an essential role in the energy-generation process during cellular respiration. It has several health benefits, such as antioxidant activity and thus can benefit human cardiovascular health. According to Health Canada (2007), a daily intake of less than 300 mg will be beneficial to cardiovascular health and provide antioxidative function. However, because of the hydrophobic nature of CoQ10, its applications in aqueous-based products are very limited. One of the potential solutions to this problem can be the adsorptive precipitation method to load it onto the PGX-processed SA as targeted in this research.

Therefore, it is hypothesized that the PGX technology can generate dried SA particles with unique morphologies, which can be used as a carrier for hydrophobic bioactive compounds, such as CoQ10. In addition, it is also hypothesized that the adsorptive precipitation process can homogeneously load the CoQ10 onto the PGX-processed SA, and thus broaden its applications in aqueous-based products.

The overall objective of this MSc thesis research was to investigate the effect of PGX process on the physicochemical properties of a water-soluble polysaccharide (specifically SA),

and use it as a carrier to load a hydrophobic bioactive compound (specifically CoQ10) by adsorptive precipitation process to improve the dispersibility and broaden the application of the hydrophobic compound in an aqueous system. To achieve this overall objective, the specific objectives were:

i) to determine the effects of SA aqueous solution concentration, mass flow rate ratio of aqueous solution:ethanol:CO_2, and flow rate of ethanol employed during PGX drying on the surface area, morphology, thermal behavior, molecular-level structure and arrangement, bulk density, and viscosity of the PGX-dried SA (Chapter 3); and

ii) to investigate the effects of circulation time and rate, operation pressure, and form of biopolymer used in adsorptive precipitation on the CoQ10 loading content, particle morphology, thermal behavior, molecular-level structure, and dispersion in an aqueous system (Chapter 4).

Chapter 2. Literature review

2.1 Sodium alginate

2.1.1 Sources and structure

Alginate is a polysaccharide widely distributed in the marine brown algae and soil bacteria, which generally serves as the structural component of the cell walls. The structures formed by the alginate provide mechanical flexibility and strength to the cells (Andresen et al., 1977). Alginate comes from abundant marine resources in nature with an approximate annual industrial production of 30,000 metric tons (Draget, 2009). The alginate products sold in the market are mainly extracted from the algae species *Laminaria japonica, Laminaria digitata, Laminaria hyperborea, Lessonia nigrescens, Eclonia maxima, Macrocystis pyrifera,* and *Ascophyllum nodosum* (Draget, 2009). On the other hand, the alginate extracted from bacteria can have unique compositions, such as alginate composed of 100% mannuronate produced by *Pseudomonas aeruginosa* (Skjaêk-brák et al., 1986). Also, the alginate extracted from bacteria is usually acetylated.

Alginate is a linear copolymer, which is composed of (1,4)-linked β-D-mannuronate (M) and α-L-guluronate (G) residues. The polymer chain is composed of consecutive M residues, alternating M and G residues, and consecutive G residues as shown in Figure 2.1. It does not have regular repeating units, which means the general monomeric composition knowledge cannot be used to determine the specific sequence of the M and G blocks in the polymer (Painter

et al., 1968; Larsen et al., 1970; Tonnesen and Karlsen, 2002). However, it is possible to use high-resolution nuclear magnetic resonance (NMR) spectroscopy to determine the frequency of M and G residues in the polymer chain based on the interactions of the proton with the adjacent electronegative groups, under the nuclear shielding environment, which enables the calculation of the average length of G blocks (Grasdalen et al, 1977; Grasdalen, 1983).

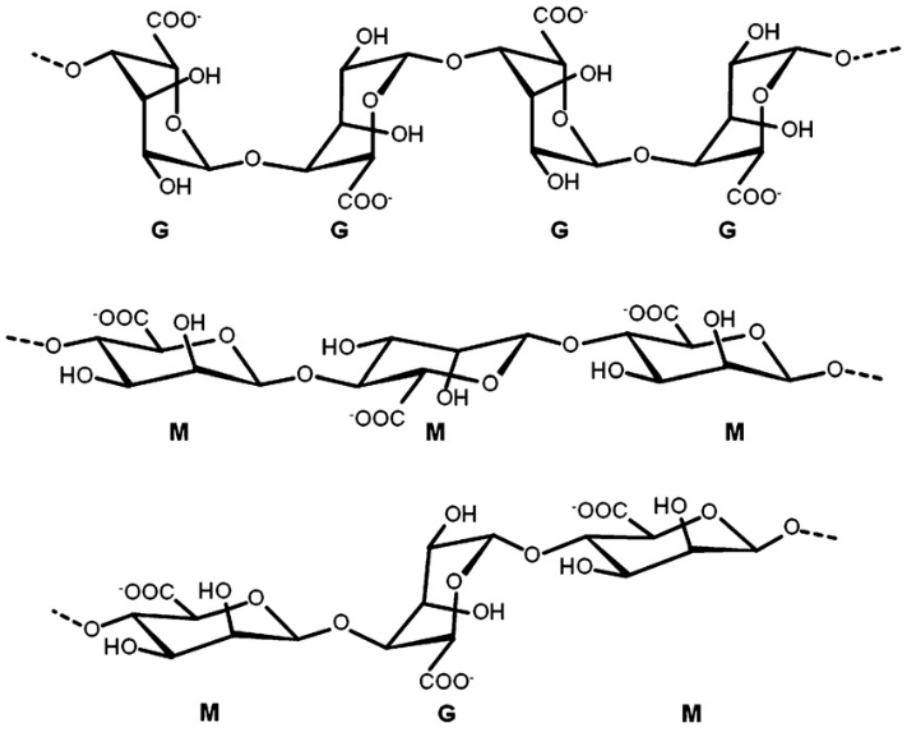

Figure 2.1 Structural characteristics of alginate: G-block (top), M-block (middle), and alternating M and G-block (bottom). Reprinted from Lee and Mooney (2012) with permission from Elsevier.

The molecular weight (MW) of the alginate is polydisperse just like most of the polysaccharides, but is generally in the range from 32,000 to 400,000 g/mol (Lee and Mooney, 2012). This is because the alginate is synthesized by polymerase enzymes but not coded by the

DNA. In addition, during the extraction process, depolymerization can happen, which would affect the MW. Therefore, the MW of the alginate is usually expressed as a range or as an average over the total distribution of the MW (Draget, 2009).

2.1.2 Extraction of sodium alginate

Alginate has been broadly used in industries and academic research because of its abundance in nature, its ability to retain water and form a gel, and its high stability. Although alginate can be produced from brown algae and bacteria, nowadays, all alginates sold commercially are produced from brown algae (Draget, 2009).

The alginate present in the brown algae is insoluble in water, which is combined with the counter ion, and in ion exchange equilibration with the surrounding seawater. Therefore, the first step in alginate extraction is using 0.1-0.2 M mineral acid to do the ion exchange with the milled algae to solubilize alginate in water in the form of alginic acid. Secondly, sodium carbonate or sodium hydroxide is used to neutralize the alginic acid, in order to obtain the sodium alginate in water solution. Then, separation processes such as filtration, or centrifugation are used to remove the other insoluble parts of the algae. The last step is to precipitate the solubilized sodium alginate out of the water solution, for which mineral acid can be applied to form alginic acid, calcium chloride can be used to form hydrogels, or alcohol can be added to the solution for solvent exchange to precipitate the polysaccharide, which is followed by separation, drying and milling to get the sodium alginate product sold commercially (Draget, 2009).

2.1.3 Physicochemical properties

Alginate is a natural anionic biopolymer and can form viscous solutions when in contact with water (Gombotz and Wee, 1998). The alginate can bind ions, which is related to its gel-forming properties, and its affinity towards different multivalent cations is based on its composition (Hang, 1964). In addition, the gelation property of the alginate is dependent on the homopolymeric G blocks; the more G residues there are in the polymer chain, the higher is the selectivity with different affinities for various alkaline earth metals (Smidsréd, 1973; 1974).

In terms of the solubility of alginate in an aqueous system, the ionic strength, pH, and the concentration of gelling ions are the three main factors. A sudden decrease in pH can result in the precipitation of the alginic acid polymers. However, the precipitation of the alginate happens at a narrow range of pH, which is affected by the sequence and composition of the polymer chain. The ones that have more alternating M and G blocks are more likely to precipitate at a lower pH than the ones that have more homopolymeric blocks because it is much easier for the polymer chains that have more homogeneous blocks to form crystalline regions and more stable structures (Haug and Larsen, 1963; Haug et al., 1967).

Dried alginate in powder form and stored at low humidity and low temperature conditions can last for a few months. However, an alginate solution has low stability because several chemical reactions can happen in the aqueous system. Both alkaline and acidic degradations, as well as free radical oxidations can happen during the storage of aqueous alginate solutions. Because alginate is extracted from natural resources, it is possible for enzymatic hydrolysis to

happen as well (Gacesa et al., 1989). Moreover, irradiation or sterilization can also cause depolymerization of the alginate (Leo et al., 1990).

2.1.4 Applications in food products

Due to its gel-forming property, and high aqueous solution viscosity, the alginate has broad applications in food products. The alginate is able to modify or improve the texture of foods since it can interact with proteins and fibers in the mixture (Sime, 1990). For example, alginate can be used as a stabilizer and affect the melting point of ice cream products (Regand and Goff, 2003). In addition, it can be used to make reconstructed food products, such as onion rings, meat chunk, pet food, fish patties, etc. Moreover, alginate is also applied in bakery products, in which it can function as a thickening agent that can make the product more heat resistant, and freeze-thaw stable (Onsøyen, 1997). In some cases, it is used in fruit jams, and some jelly products, due to its thickening and gel-forming properties (Toft et al., 1986).

Some researchers used alginate as a carrier for nutrients or bioactive compounds to fortify food products. For example, Pranoto et al. (2005) incorporated garlic oil in alginate films for antibacterial fortification of food products. Alboofetileh et al. (2014) used alginate to make nanocomposite films containing essential oils for controlling the growth of foodborne pathogens. Moreover, alginate is also used to make active food packages for different purposes, such as antimicrobial and antioxidant functions. Bierhalz et al. (2012) made an active film for food packaging by using alginate and pectin mixture incorporated with natamycin to prevent the

growth of harmful food microorganisms. Rhim (2004) made calcium chloride modified sodium alginate film to resist water for food packaging applications.

2.2 Coenzyme Q10

2.2.1 Sources and structure

Coenzyme Q10 is a 2,3-dimethoxy, 5-methyl, 6-polyisoprene parabenzoquinone as shown in Figure 2.2. The coenzyme Q10 (CoQ10) has ten isoprene units in its polyisoprene chain (Crane, 2001). The CoQ10 has been found in each cell and mitochondria membranes of aerobic respiration organisms, and plays an essential role during energy generation, and maintaining cellular functions (Saini, 2011).

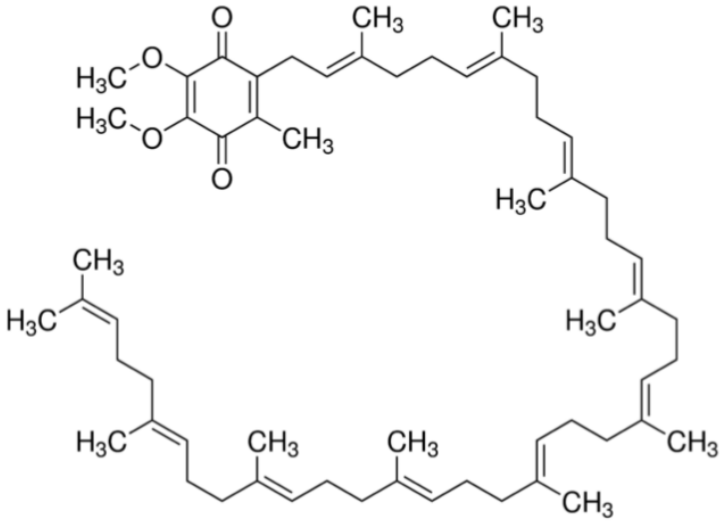

Figure 2.2 Chemical structure of CoQ10.

CoQ10 plays an important role during the adenosine triphosphate (ATP) production process. Most ATPs are generated in the inner membrane of the cell mitochondria. CoQ10 serves as a

proton transfer medium, and then forms the proton gradient from the inside to the outside of the mitochondria membrane. Then ATP is formed from adenosine diphosphate (ADP), and the protons are combined with the oxygen to form water at the end of the oxidative phosphorylation process. During this process, the CoQ10 can be in the state of semiquinone or quinone when semi or fully oxidized, respectively. In addition, it can be turned into the quinol form after the reduction process as shown in Figure 2.3 (Yamamoto and Yamashita, 1997; Brandt, 1999).

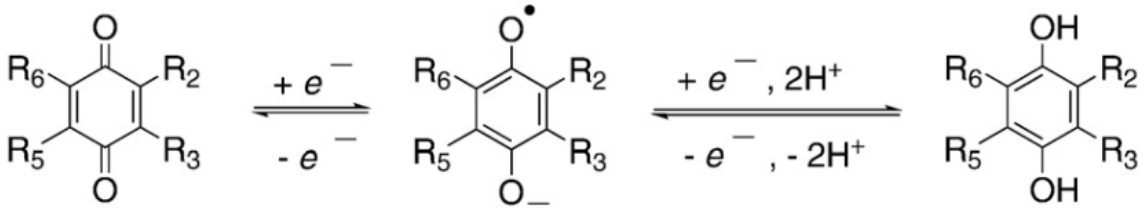

Figure 2.3 Chemical structure of quinones, semiquinones, and quinols. Reprinted from Song and Buettner (2010) with permission from Elsevier.

CoQ10 is a good antioxidant as well. Inside of the membrane system, most of the CoQ10 is in the quinol form, which is the reduced form that can be easily oxidized and turn into the semiquinone or quinone form (Takahashi et al., 1993). Therefore, it can react with the oxygen and free radicals of lipids and provide health benefits to the organism. Hoppe et al. (1999) applied skin cream containing CoQ10 on elder human skin, and demonstrated that CoQ10 resulted in a substantial decrease of luminescence free radicals. Moreover, apart from its own antioxidant function, CoQ10 can also reduce the tocopheryl radicals, and speed up the regeneration of tocopherol in the organisms (Arroyo et al., 2000).

Because CoQ10 is present in the cell membrane of the aerobic respiration organisms, many

animal-based products and some plant-based resources can be used as the source of CoQ10. For example, all of the pork, chicken, beef, fish, and lamb products, especially the viscera parts, have a large CoQ10 content. Specifically, the pork heart contains the most CoQ10 in the meat-based products, which is around 203 μg/g, whereas the content in the beef heart can be up to 41 μg/g (Lester and Crane, 1959). Some plant-based products such as spinach (2.3 μg/g) and orange (2.2 μg/g) also contain CoQ10 (Lester and Crane, 1959); however, the CoQ10 levels in plant-based products are usually low, because this hydrophobic compound is generally coupled with fat, and is present in the parts that contain a high amount of mitochondria.

The current commercial CoQ10 production methods are mainly based on chemical synthesis and microbial production (Jeya et al., 2010), which can achieve a CoQ10 production scale from 350 to 770 mg/L (Ha et al., 2007). In addition, the CoQ10 is usually extracted and purified by using organic solvents such as hexane and *n*-propanol, followed by the purity determination using high-performance liquid chromatography (Jeya et al., 2010).

2.2.2 Health benefits

CoQ10 has many health benefits due to its unique functional and structural characteristics. Based on the information provided by Health Canada (2007), CoQ10 can benefit human cardiovascular health, reduce the frequency of migraine headaches, and can be used as an antioxidant. Using 30 to 300 mg of CoQ10 per day will have a positive effect on cardiovascular health, while a daily intake of 150 to 300 mg can reduce the occurrence of migraine prophylaxis, and less than 300 mg per day can provide antioxidant function to human bodies (Health Canada,

2007).

Many diseases happen due to the accumulation and action of reactive oxygen species (Battino et al., 2001). The CoQ10 can function as an antioxidant to decrease the amount of free radicals inside the organisms. However, there is only 500 to 1500 mg of CoQ10 inside the whole human body, which starts to decrease with age (Hoppe et al., 1999). In addition, various diseases can result in a decrease of CoQ10 in some tissues and serum as well, which is not possible to be increased significantly by the normal daily diet (Crane, 2001). Therefore, it is recommended to take supplements.

CoQ10 can be applied to benefit against cardiovascular diseases, such as hypertension, chronic heart failure, etc. These health benefits are related to its important role in energy generation, the ability of antioxidation of low-density lipoproteins in the plasma, and its ability to regulate the channels in the cell membrane system (Bank et al., 2011). A few clinical studies focused on the efficacy and safety of applying CoQ10 against hypertension, which proved that CoQ10 was able to lower the blood pressure and it was safe to be applied to the patients (Wyman et al., 2010). Moreover, CoQ10 is able to reverse mitochondrial dysfunction, and can be used to minimize the side effects of some cancer treatments (Nicolson and Conklin, 2008). Hertz and Lister (2009) focused on the survival of late-stage cancer patients, and used CoQ10 and other antioxidants as supplements during the treatment. It was found that 76% of the patients survived longer than the anticipated survival period.

Since CoQ10 is a hydrophobic bioactive compound, it can be better absorbed by the human

body when consumed together with meals containing oil. However, it cannot function immediately after the intake, which may take up to eight weeks in order to provide its health benefits (Saini, 2011). Nowadays, there are many CoQ10 supplements on the market, which are sold in the form of tablets, capsules, soft gels, and powders; however, formulation of such products is challenging considering the crystalline and hydrophobic nature of CoQ10.

2.3 Polysaccharide drying methods

2.3.1 Traditional methods

The natural polysaccharide materials are commonly used in food and pharmaceutical industries because of their functional properties, such as gel-forming, high viscosity in aqueous systems, and potential to be used as stabilizers, as well as the high biocompatibility with other food ingredients and biomaterials. In addition, the abundant polysaccharide resources in nature make the product low cost as well (Bhardwaj et al., 2000; Vendruscolo et al., 2009).

As ingredients, polysaccharides are generally sold in powder form. Therefore, they need to be dried after extraction from their original source materials. Many techniques have been applied for the drying of polysaccharides, such as spray drying, freezing drying, air drying, and microwave drying (Nep and Conway, 2011). However, all drying methods have the possibility to affect the original physicochemical properties of the polysaccharides (York, 1983). In addition, it is very challenging to handle highly viscous high molecular weight polysaccharides, especially in spray drying.

Nep and Conway (2011) focused on the effect of drying method on the properties of Grewia polysaccharide gum, which was extracted from the inner stem bark of *Grewia mollis*, an edible plant from Nigeria. Air drying, freeze drying, and spray drying were performed under the following conditions: air drying was performed in an oven at 50 °C for 24 h, spray drying was at 160 °C, and freeze drying was at -40 °C for 72 h. The results showed that the viscosity of the dried Grewia gum was different for each drying method, which might be because the processing temperature and shear affected the molecular weight.

Kong et al. (2015) compared the effect of vacuum drying and freeze drying on the physicochemical properties of polysaccharide extracted from *Bletilla striata,* which has been used in Chinese herbal medicine for a long time. The extracted polysaccharide was first precipitated by 70% ethanol followed by centrifugation, and then the precipitate was re-dissolved in water for drying where freeze drying was performed at -60 °C for 24 h, and vacuum drying was carried out in a vacuum oven for 72 h. The results showed that the freeze dried sample had better solubility, lower aggregation, and lower thermal stability, and there was a clear difference between their morphologies.

2.3.2 Supercritical CO_2-based methods

Supercritical carbon dioxide (SC-CO_2) is CO_2 at pressure and temperature conditions beyond its critical point (31.1 °C, 73.8 bar). In the supercritical region, the CO_2 exhibits both liquid-like and gas-like properties, including high diffusivity and high solvent power. In addition, the SC-CO_2 properties can be easily tuned by manipulating the pressure and temperature. Based

on the unique properties of SC-CO_2, it is already being used in many research areas and applications, such as valuable compound extractions, bioactive material enrichments, and encapsulations (Brunner, 2005), as well as its use as the medium for different reactions, and as a reprocessing fluid for fibers and particles (Yeo and Kiran, 2005).

The supercritical fluid drying method has been applied for drying of polysaccharides or their aerogels. For the drying of aerogels, solvent exchange is applied first prior to the drying process, where ethanol is usually used to convert hydrogel into an alcogel, and then SC-CO_2 can be applied for the extraction of ethanol to obtain aerogel. Comin et al. (2012) focused on making barley β-glucan aerogels by using the SC-CO_2 drying method. In addition, air drying and freeze drying were also applied for comparison with the SC-CO_2 drying. It was shown that SC-CO_2 method could result in lower density and uniform morphology of the interior gel structure.

Many biopolymer processing and drying methods have been developed over the years, as reviewed by Yeo and Kiran (2005). For example, the rapid expansion of supercritical solutions (RESS) is used for the polymers, which can dissolve in the supercritical fluid, followed by a rapid depressurization to achieve the precipitation of the biopolymer (Debenedetti et al., 1993). The gas-antisolvent process (GAS) requires the polymer to be insoluble in the supercritical fluid, where the polymer is first dissolved in an organic solvent, and then the supercritical fluid is passed through the solvent to serve as the antisolvent and precipitate the polymer (Park and Yeo, 2008). Moreover, the supercritical antisolvent process (SAS) involves spraying the polymer solution into the high-pressure chamber, which has been previously filled with the supercritical

fluid. After the contact between the streams, rapid precipitation and growth of the polymer particles begin, and then particles with unique morphologies are formed (Yeo et al., 1993). In some cases, an organic solvent, such as ethanol can be used together with the supercritical fluid to serve as an antisolvent, and then an aqueous-based polymer can be processed and dried by using the SAS technology. The particles from gas saturated solutions (PGSS) is another biopolymer processing technology based on the application of supercritical fluids. The supercritical fluid is first dissolved in the molten polymer or its liquid suspension and then sprayed through a nozzle for rapid depressurization to precipitate the polymer material (Martín et al., 2010).

Another recently developed method, targeting the processing of water-soluble biopolymers is pressurized gas expanded liquid (PGX) technology (Temelli and Seifried, 2016). This process is based on the antisolvent principle, which is performed by first stabilizing the high-pressure vessel to a certain pressure using the mixture of SC-CO_2 and ethanol, and then the aqueous biopolymer solution is pumped in and mixed with the SC-CO_2 and ethanol mixture at the tip of a co-axial nozzle, resulting in the precipitated biopolymer. After completion of pumping of the aqueous polymer solution, SC-CO_2 and ethanol mixture is continued to be pumped to remove the water residue, and then only SC-CO_2 is pumped in for ethanol removal from the system, followed by depressurization and collection of the dried product (Seifried, 2010).

The operational parameters are selected in such a way that when the three streams (CO_2, ethanol, and biopolymer solution) of the PGX process are combined, they form a single liquid

phase during the process, which is based on the ternary phase equilibria (Durling et al., 2007). Figure 2.4 shows the ternary phase diagram water-ethanol-CO_2 and the phase boundary at different pressures and 40 °C. The one-phase region above the phase boundary on the ternary diagram is composed of expanded-liquid region (above the mixture critical point) and supercritical fluid region (below the mixture critical point), and the PGX process is based on the conditions in the expanded-liquid region.

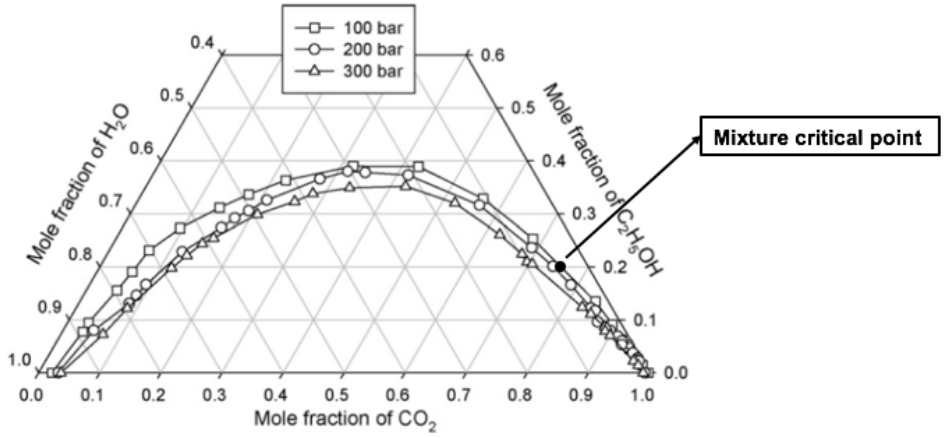

Figure 2.4 Ternary phase diagram for water-ethanol-CO_2 mixture at 40 °C. Reprinted from Durling et al. (2007) with permission from Elsevier.

Another technique is expanded liquid antisolvent (ELAS) process, which was reported later and is similar to the PGX process, which uses the mixture of CO_2 and an organic solvent in the expanded-liquid region as the antisolvent to precipitate the water-soluble biopolymer at constant pressure and temperature (Prosapio et al., 2014). They employed the ELAS technology for the drying of bovine serum albumin, rather than the water-soluble polysaccharides. The basic principles of the PGX and ELAS are similar, but some operational procedures are different. For

example, they pressurized the system by only applying CO_2 first, and then the co-solvent such as ethanol was pumped and mixed with CO_2 to form the expanded liquid, followed by pumping the aqueous polymer solution to perform the drying process.

Bouchard et al. (2008) reported drying carbohydrates by using the conditions in the supercritical fluid region of the ternary diagram. The drying process was similar to the PGX process in terms of the use of CO_2 and ethanol mixture to precipitate the carbohydrates from an aqueous solution at the tip of a co-axial nozzle, followed by water and ethanol removal to obtain the dried product. However, by using the conditions in the supercritical fluid region, they were not able to obtain dry powders of the polysaccharides such as inulin.

2.4 Delivery systems involving sodium alginate and CoQ10

2.4.1 Traditional delivery methods for CoQ10

Since CoQ10 is a hydrophobic bioactive compound with high molecular weight and crystalline nature, it is very challenging to incorporate it into aqueous-based products, including food and beverage products, and only a limited amount of CoQ10 can be absorbed and used by the human body after direct ingestion of such aqueous products. On the other hand, if a CoQ10 supplement is taken together with normal daily diet containing lipids, then the human body can adsorb and uptake it more efficiently (Barakat et al., 2013). In addition, since the CoQ10 has high permeability but low solubility, and the highest CoQ10 permeability exists in the duodenum and colon, a specific delivery system and a fast drug release is required for the CoQ10

supplements (Palamakula et al., 2005).

Several incorporation and delivery methods have been investigated for CoQ10, in order to enhance its applications in aqueous-based products, increase its bioavailability, and protect it from the outside environment. For example, self-emulsifying drug delivery system (Kommuru et al., 2001), binary solid dispersion (Bhandari et al., 2007), emulsification (Kwon et al., 2002), lipid carrier (Chen et al., 2013), direct dispersion of CoQ10 into the polysaccharide (amylomaize starch and its dextrin) aqueous solution (Kim et al., 2012), and encapsulation (Cheuk et al., 2015) are some of the approaches investigated.

Some traditional emulsification methods were broadly applied, such as the polymerization process (Couvreur and Vauthier, 1991), but due to the toxic residues inside the product, its application has been limited. In addition, the spontaneous interfacial deposition method has been applied to incorporate a hydrophobic bioactive compound into the pre-formed polymer. However, this technology could result in the aggregation of the bioactive compounds (Espuelas et al., 1997). Therefore, high-pressure homogenized emulsions were prepared by using a microfluidizer, which could solve the traditional emulsification problems mentioned above (Kwon et al., 2002). Using such an approach, CoQ10 was loaded in the poly-(methyl methacrylate) to make nanoparticles, where the process was easy to manipulate, and a high CoQ10 loading amount of 38.7% (w/w) and a highly stable product were obtained (Kwon et al., 2002).

Bhandari et al. (2007) focused on making a binary solid dispersion to enhance the solubility of CoQ10 in an aqueous system. Poloxamer 188 and CoQ10 were mixed at different weight

ratios, melted, and cooled to obtain the binary solid dispersion. The dispersibility of CoQ10 was highly increased by applying such a binary solid dispersion method. In addition, performing this process at a temperature between 70 and 80 °C did not affect the properties of CoQ10. Moreover, the binary solid dispersion product resulted in a fast release of the bioactive compound based on their *in vitro* study.

Kim et al. (2012) focused on making CoQ10 aqueous dispersion in starch or its dextrin solution. First, the starch or dextrin solution was prepared, and then CoQ10 was added and stirred at 60 to 80 °C for 3 days, with the application of a 3 min ultrasonication every 6 h. After that, a 12-h cooling period followed by centrifugation was applied to obtain the precipitated product. They also performed redispersion and ultrasonication of the precipitates, in order to compare the particle size and stability. In the end, it was possible to obtain the CoQ10 aqueous dispersion with water-soluble polysaccharides, without adding emulsifiers, and the ultrasonication helped to reduce the particle size and stabilize the CoQ10 dispersion.

Sodium alginate is a long-chain polysaccharide, which can absorb water, form gels, and stabilize an aqueous system. Therefore, it has a broad application for use as a carrier and make delivery systems for bioactive and valuable compounds. In many cases, alginate beads are used to serve as the carrier for drug delivery, and it can also be used as the coating material in various encapsulation techniques (Tønnesen and Karlsen, 2002). For example, to make encapsulated drug delivery systems using alginate, the aqueous system with hydrophobic indomethacin suspension was firstly prepared, followed by spray drying to obtain the product. The drug release

rate could be controlled by adjusting the wall thickness of the alginate coating material, or by adding some other linkage or compounds to modify the wall structure (Joseph and Venkataram, 1995).

Alginate beads can be used to prepare delivery systems for proteins and other kinds of macromolecules, since alginate is able to form gels and incorporate the macromolecules without applying organic solvents (Patil and Speaker, 1997). Based on the pore structure and properties of the alginate gel, it is possible to achieve an ideal control of the release of the compounds incorporated (Bhardwaj et al., 2000).

Cyclodextrin complexes were also applied to load CoQ10 to increase its solubility in the aqueous system. Gao et al. (2006) employed four different forms of cyclodextrin to incorporate CoQ10 by using the solvent evaporation method. The γ-cyclodextrin complex increased the CoQ10 dissolution rate significantly, and the bioavailability study of this γ-cyclodextrin complex in dogs showed that its maximum concentration was 1.24 times higher than that of pure CoQ10 (Gao et al., 2006).

2.4.2 Adsorptive precipitation method

The adsorptive precipitation process for loading of bioactives and drugs is composed of two steps. The first step is the adsorption of the bioactive compound on the surface of the carrier system based on their affinity, and the second step is the precipitation of the bioactive compound out of the solvent stream based on the loss of solubility upon change of conditions or the evaporation of the solvent. The solvent should be able to solubilize the bioactive but not the

carrier material, and therefore, SC-CO_2 is usually used as the solvent and as the media to achieve loading of bioactive on the biopolymer carrier (Gurikov and Smirnova, 2018).

During the adsorptive precipitation process, a bioactive in crystalline form can be transformed to amorphous form after the loading process, which would enhance its bioavailability. The crystalline compound can be either transformed by direct conversion or turned into its non-crystalline form after being melted and solubilized into the solvent stream.

In most cases, a solid porous biopolymer is used as the carrier and loading matrix for the hydrophobic bioactive compound, and a high surface area is usually preferred due to its potential for loading of a high amount of bioactive or drug onto it. In addition, SC-CO_2 has many advantages for serving as the solvent, because it is non-toxic, chemically stable, and has moderate processing conditions to reach the supercritical fluid region. However, some drugs and bioactive compounds are not highly soluble in SC-CO_2; therefore, some co-solvents, such as anhydrous ethanol is generally used to increase the solvent power towards more polar compounds. On the other hand, if organic solvents are included in the adsorptive precipitation process, it can result in a wet product or bioactive being washed out during the depressurization step.

Static and dynamic adsorptive precipitation processes are used. The static process involves putting the bioactive and carrier material together in a high-pressure vessel, and allowing time for the saturation of SC-CO_2; after reaching the adsorption equilibrium, depressurization step is applied to finish the precipitation process. On the other hand, the dynamic process is achieved by

placing the two components separately, saturating the SC-CO_2 with the bioactive, and then carrying the bioactive to the biopolymer vessel to achieve adsorption equilibrium, followed by depressurization to finish the precipitation. During the process, operation temperature, pressure, and depressurization rate are the main factors, which affect the solvent power of the SC-CO_2, and the adsorption on the biopolymer. The depressurization rate can affect the speed and time for the precipitation of the bioactive compound coming out of the solvent stream and loading on the biopolymer carrier.

A few studies focused on making bioactive fortifications or delivery systems by using the adsorptive precipitation process. For example, Couto et al. (2018b) loaded CoQ10 on PGX-processed β-glucan. A dynamic flow system that was able to recirculate the SC-CO_2 + CoQ10 through the β-glucan bed was used. The effects of recirculation time and SC-CO_2 flow rate, as well as the depressurization rate at the end of the process were investigated. They found that as the adsorption time was increased, the adsorbed CoQ10 amount first increased and then decreased, which was because the CoQ10 might be redissolved into the SC-CO_2 stream after the peak adsorption. In addition, they found that a faster depressurization rate could lead to a higher amount of CoQ10 being precipitated quickly. The highest CoQ10 loading of 17.5 % (w/w) was obtained at 45 min of adsorption time, and depressurization rate of 130 bar/min (Couto et al., 2018b).

Gorle et al. (2010) focused on achieving adsorption of benzoic acid on different aerogel carriers. The static process was performed by loading aerogel together with the benzoic acid in a

high-pressure view cell. Then, CO_2 was introduced into the cell and maintained at the targeted processing condition for 24 h, followed by a slow depressurization. It was found that the loading amount was related to the adsorptive properties of different carriers, and the aerogel with a polar surface adsorbed more benzoic acid (Gorle et al., 2010). In addition, the crystallinity of the benzoic acid was also affected by the surface interactions with the silica aerogels.

There is growing interest on loading hydrophobic bioactive compounds on polymeric carriers using the adsorptive precipitation method. However, there is lack of information on the adsorptive precipitation of CoQ10 on alginate-based biopolymers. Therefore, in the following chapters, PGX drying of SA was firstly investigated (Chapter 3), followed by adsorptive precipitation of CoQ10 on PGX-processed SA (Chapter 4).

Chapter 3. Drying of sodium alginate using Pressurized Gas eXpanded (PGX) liquid technology

3.1 Introduction

Sodium alginate (SA) is a polysaccharide, which is extracted from brown algae and is composed of (1-4) linked β-D-mannuronic acid and α-L-guluronic acid units. SA is a hydrophilic compound that generally has a molecular weight ranging from 32,000 to 400,000 g/mol (Lee and Mooney, 2012). Because it comes from an abundant marine resource and it has unique physicochemical properties, it has broad applications, including food, biomedical and other applications. When SA is used as a bioactive delivery system, in most cases it is in the form of a hydrogel. However, there is lack of information for the use of dried SA as a delivery system. Due to its long-chain structure, high molecular weight, strong hydrophilic properties and high viscosity, it is challenging to dry such polysaccharides using conventional drying methods.

Supercritical carbon dioxide (SC-CO_2) can be used for polymer drying and particle formation. When CO_2 is mixed with water and an organic solvent, such as anhydrous ethanol (EtOH) at certain ratios, and pressurized, this mixture can be in a single liquid phase, depending on phase equilibria (Chiu et al., 2008), which is referred to as gas-expanded liquid.

The Pressurized Gas eXpanded liquid technology invented by Temelli and Seifried (2016) is based on the anti-solvent method and able to dry high molecular weight biopolymers from aqueous solution, resulting in unique morphologies, which are not possible to achieve by other drying methods. The PGX technology operates at moderate conditions (for example 40 °C and

100 bar), using food grade anhydrous ethanol and carbon dioxide (CO_2) mixture as the drying medium. This technology has already been applied to dry β-glucan and gum arabic, resulting in efficient drying and high surface area of the product (Seifried, 2010). Therefore, this technology has a likely potential to dry SA and result in a high surface area product as well. Indeed, Seifried (2016) has mentioned the formation of a high surface area SA powder using PGX technology; however, the impact of different PGX processing parameters on the drying of SA has not been reported previously. Therefore, The objective of this study was to investigate the effect of different processing parameters (SA aqueous solution concentration, mass flow rate ratio of aqueous solution:ethanol:CO_2, and flow rate of ethanol) on the physicochemical properties (surface area, morphology, thermal behavior, molecular-level structure and arrangement, bulk density, and viscosity) of PGX-dried SA.

3.2 Materials and methods

3.2.1 Materials

The alginic acid sodium salt (product No. 180947, molecular weight 120,000-190,000 g/mol) was purchased from Sigma-Aldrich (Oakville, ON, Canada), which was extracted from brown algae and it was in powder form. Anhydrous ethanol (> 99.5%) was purchased from Greenfield Global Inc. (Brampton, ON, Canada). Carbon dioxide (99.9% purity, < 3 ppm H_2O) was purchased from Praxair Canada Inc. (Mississauga, ON, Canada).

3.2.2 PGX unit

The flow chart of the PGX unit is shown in Figure 3.1. A Thar SFE 500 unit (Waters, Milford, MA, USA) was modified with the addition of a third liquid pump (600E, Waters, Milford, MA, USA) to pump in a third stream (aqueous polymer solution). In addition, a modified tubing setup with a co-axial nozzle at the end was inserted at the top part of the 500 mL collection vessel for the inlet of EtOH+CO_2 mixture in the outer tube and the aqueous polymer solution in the inner tube to achieve the mixing of the two streams. In addition, a custom-made basket (stainless steel, with 4.48 cm internal diameter, 5.35 cm external diameter, and 19.05 cm height) was fitted inside the collection vessel and three felt filters (polyester felt, pore size 5 μm, McMaster-Carr, Aurora, OH, USA) were placed on the metal holder at the bottom of the basket for collecting the dried SA particles. O-rings placed around the basket ensured the flow of fluids through the basket.

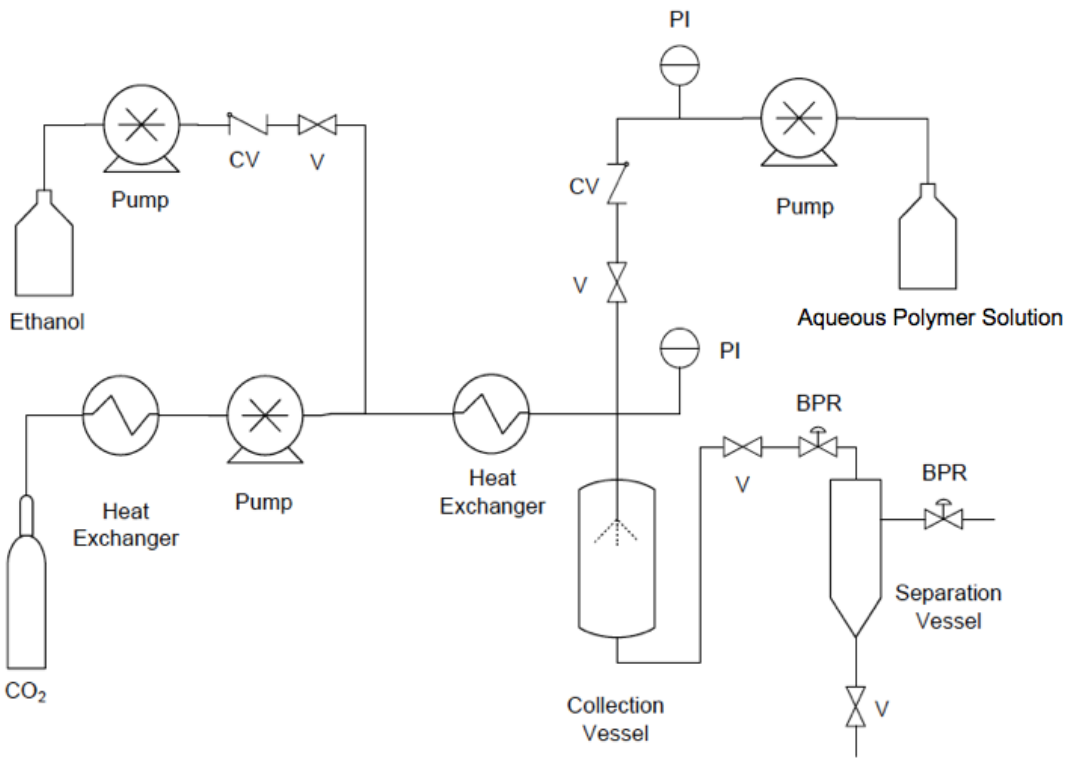

Figure 3.1 Flow chart of the PGX unit. CV: check-valve; V: valve; PI: pressure gauge; BPR: back pressure regulator.

The whole system was first heated up and stabilized at 40 °C. During this period, SA aqueous solution was prepared by mixing a certain amount (3.0, 4.5, and 6.0 g) of "unprocessed" SA powder (as received from the supplier) with 300 mL deionized water using a magnetic stirrer at 40 °C, and then the prepared SA aqueous solution was centrifuged by using Corning LSE compact centrifuge (Corning Inc., Corning, NY, USA) at 4185 × *g* for 10 min, in order to remove the insoluble fraction. Due to its high molecular weight, SA dispersed in water forms a colloidal solution (sol). Then, the supernatant was used as the aqueous polymer solution feed for the PGX process. Then, the unit was pressurized to the target pressure by pumping the CO_2 and EtOH mixture at a certain ratio. The liquid was collected every 5 min from the separation vessel. After

the pressure was stabilized, the aqueous SA solution was pumped in and mixed with the EtOH and CO_2 at the tip of co-axial nozzle, and the liquid went through into the separation vessel. CO_2 + EtOH served as an anti-solvent to precipitate the polymer from the aqueous solution stream, as well as a solvent for the removal of water. After delivering a targeted amount (40 mL) of solution, the aqueous solution pump was stopped and CO_2 + EtOH mixture was continuously pumped in order to remove the water residue inside the collection vessel. Then, only CO_2 was pumped in to dry the EtOH residue inside the system. Once there was no more liquid coming out of the separation vessel, CO_2 was continued to be pumped at a flow rate of 40 g/min for another 45 min, which was equivalent to three times the volume of the collection vessel to sufficiently dry the SA biopolymer. Finally, the whole system was slowly depressurized to ambient pressure to remove the dried biopolymer, collected on the filter placed at the exit of the basket inside the collection vessel.

3.2.3 Experimental design

Three different parameters were tested in this study (Table 3.1), which include SA aqueous solution concentration (1.0, 1.5, and 2.0% w/w), EtOH mass flow rate (15, 24, and 30 g/min), and mass flow rate ratio (1:6:2, 4:15:5, and 1:3:1 of SA solution: EtOH: CO_2). The mass flow rate ratio of EtOH and CO_2, which formed the drying fluid was kept constant at 3:1, while the mass flow rate ratio of the drying fluid to the SA solution (θ) ranged from 4:1 to 5:1 and 8:1. All the experiments listed in Table 3.1 were performed at 100 bar and 40 °C in duplicate. This mild

processing temperature and pressure condition was adopted because this condition has been applied to β-glucan and gum arabic successfully previously (Seifried, 2010), and it would allow comparisons between different water-soluble biopolymers to investigate the effect of PGX technology on their physicochemical properties.

Table 3.1 Experimental conditions tested for PGX drying of SA

Experiment	Aq. Sol Concentration (% w/w)	Aq. Sol flow rate (g/min)	EtOH flow rate (g/min)	CO_2 flow rate (g/min)	θ
1	1.0	2.5	15	5	8
2	1.0	4.0	15	5	5
3	1.0	5.0	15	5	4
4	1.0	4.0	24	8	8
5	1.0	6.4	24	8	5
6	1.0	8.0	24	8	4
7	1.0	5.0	30	10	8
8	1.0	8.0	30	10	5
9	1.0	10.0	30	10	4
10	1.5	4.0	15	5	5
11	2.0	4.0	15	5	5

θ = Mass flow rate ratio of drying fluid (EtOH:CO_2 3:1 w/w) to aqueous polymer solution

The experimental conditions were shown on the ternary phase diagram of water: ethanol: CO_2 as depicted in Figure 3.2. Three different mass ratios were tested in this study, which were presented as the mass flow rate ratio in the experimental design (Table 3.1). These three ratios

were all in the gas-expanded liquid region above the phase boundary, which was a single liquid phase of three components: water, EtOH, and CO_2. These three conditions were chosen because previous studies on β-glucan using this PGX technology (Seifried, 2010) were performed with the 1:3:1 mass ratio. Therefore, the 1:3:1 mass ratio was also applied to the SA for comparison. Moreover, two more conditions were tested by increasing the ratio of the drying fluid to aqueous SA solution to evaluate its impact on the characteristics of the PGX-processed SA.

Spray drying of SA was also performed in order to compare with the PGX-processed SA product. The 1.0% w/w SA solution was spray dried by using the LabPlant SD-06 Spray Dryer (Labplant, North Yorkshire, UK), located at the Agri-Food Discovery Place, University of Alberta. The spray drying was performed with the inlet air temperature at 175 °C, 10 mL/min SA solution feed rate, and 90 °C outlet air temperature. As a commonly used conventional technique, spray drying was selected for comparison with the PGX drying of SA because both of these processes involve a spray step, and drying is performed in a dynamic mode. The processing parameters for spray drying were adopted from a previous study on the spray drying of sodium alginate composite (Takeuchi et al., 1998).

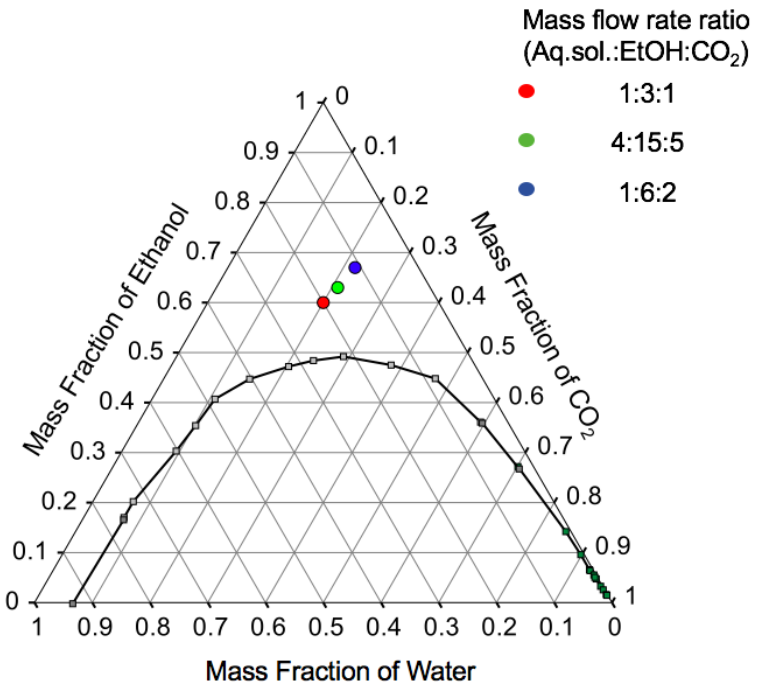

Figure 3.2 Ternary diagram of water, EtOH, and CO_2 at 100 bar and 40 °C. Data for plotting this ternary diagram was obtained from Durling et al. (2007).

3.2.4 Characterization of SA particles

Properties of 'unprocessed' (as received, before PGX processing) and 'PGX-processed' (after PGX processing) particles were determined for detailed characterization and some properties were compared to those of 'spray-dried' particles as described below.

3.2.4.1 Viscosity measurement

The viscosity of unprocessed SA, and PGX-processed SA solutions were determined using a rheometer (Discovery HR-1, TA Instrument, Mississauga, ON, Canada) equipped with a cup (Peltier Concentric Cylinder) and bob attachment. In addition, a cup cover was applied during the measurement to prevent water evaporation from the SA solution. The shear rate was varied from 1.217 to 121.7 s^{-1} at 20 °C. Moreover, the temperature effect on viscosity was determined

from 20 to 60 °C with a constant shear rate of 50 s^{-1}. Aqueous solutions of unprocessed SA at 0.5, 1.0, 1.5, and 2.0% w/w, and PGX-processed SA at 0.5% w/w were prepared for the measurement.

3.2.4.2 Particle morphology

The morphology of unprocessed and PGX-processed SA was examined by using Zeiss Orion Helium Ion Microscope (Ostalbkreis, BW, Germany), which was located at NanoFab, University of Alberta. Secondary electron images were collected at 30 kV accelerating voltage and 1.5 pA beam current. In addition, an electron flood gun was used to neutralize positive charges on the surface of the samples, which made it possible to directly take images of insulating materials without coating.

3.2.4.3 Surface area analysis

The surface area of unprocessed, PGX-processed, and spray dried SA was measured by using AutoSorb iQ (Quantachrome Instruments, Boynton Beach, FL, USA) based on nitrogen adsorption/desorption isotherm. All of the samples were degassed at 40 °C. Data were analyzed by AutoSorb iQ software using Brunauer–Emmett–Teller (BET) method.

3.2.4.4 Differential scanning calorimetry (DSC) analysis

Thermal behavior of unprocessed and PGX-processed SA was determined by using a DSC Q2000 system (TA Instruments, Mississauga, ON, Canada) calibrated with indium standards. Approximately 4 to 6 mg sample was placed into an aluminum pan for each measurement, and an empty pan was used as the blank. Measurements were carried out at the heating rate of

5 °C/min from -20 to 250 °C, with a modulation of +/- 1.00 °C every 60 s^{-1}. Data were interpreted by using Advantage software.

3.2.4.5 Fourier-transform infrared (FTIR) spectroscopy analysis

FTIR measurement was performed by using iS50 FTIR Spectrometer (ThermoFisher Scientific, Waltham, MA, USA) with a built-in attenuated total reflection (ATR) module. The ambient environment was used as the background, scanning from 400 to 4000 cm^{-1}, and 32 scans were applied to each sample.

3.2.4.6 X-ray diffraction analysis

Unprocessed SA and PGX-processed SA were examined by using Bruker D8 Discover diffraction system (Bruker, Billerica, MA, USA), equipped with Cu-source and high throughput LynxEYE 1-dimensional detector. Measurements were carried out at a voltage of 40 kV and 30 mA. All the samples were continuously scanned from 5 to 75° at 5° 2θ per minute. Data were analyzed by using JADE 9.6 software.

3.2.4.7 Bulk density measurement

The bulk density measurement of PGX-processed SA sample was performed by determining the volume from the height and diameter of the entire sample placed in a glass vial, and measuring the weight by using an analytical balance (AB204-S, Mettler-Toledo Ltd., Leicester, UK). In addition, the volume of the unprocessed and spray-dried SA was measured by using a 10 mL graduated cylinder without tapping, and the weight was measured by the same analytical balance.

3.2.4.8 Statistical analysis

Statistical analysis of data was performed using RStudio 1.1.383 (R Core Team, 2015). One-way analysis of variance (ANOVA) was performed for the bulk density measurement, and means were compared by using paired t-test of least square means with significance difference defined at $p < 0.05$.

3.3 Results and discussion

3.3.1 Viscosity measurement

It is important to understand the viscosity behavior of the aqueous polymer solution since it affects the mixing with the drying fluid during processing. The viscosity measurement results presented in Figure 3.3 indicated that viscosity increased as the concentration of SA in the aqueous solution increased, which was as expected. In addition, with an increase in the shear rate, the viscosity of all SA solutions showed shear-thinning behavior at lower shear rates, and approached a constant viscosity value as shear rate increased.

The viscosity behavior of the 0.5% PGX-processed SA was similar to that of the 0.5% unprocessed SA, which indicates that the polymer chain length or the molecular weight was not affected by the PGX drying process. Donnan and Rose (1950) reported the relationship between molecular weight and viscosity of sodium alginate, and they found that the molecular weight had a linear relation with the intrinsic viscosity. Therefore, if the molecular weight of the SA was affected by the PGX process, the viscosity would have been different when compared with the

unprocessed material.

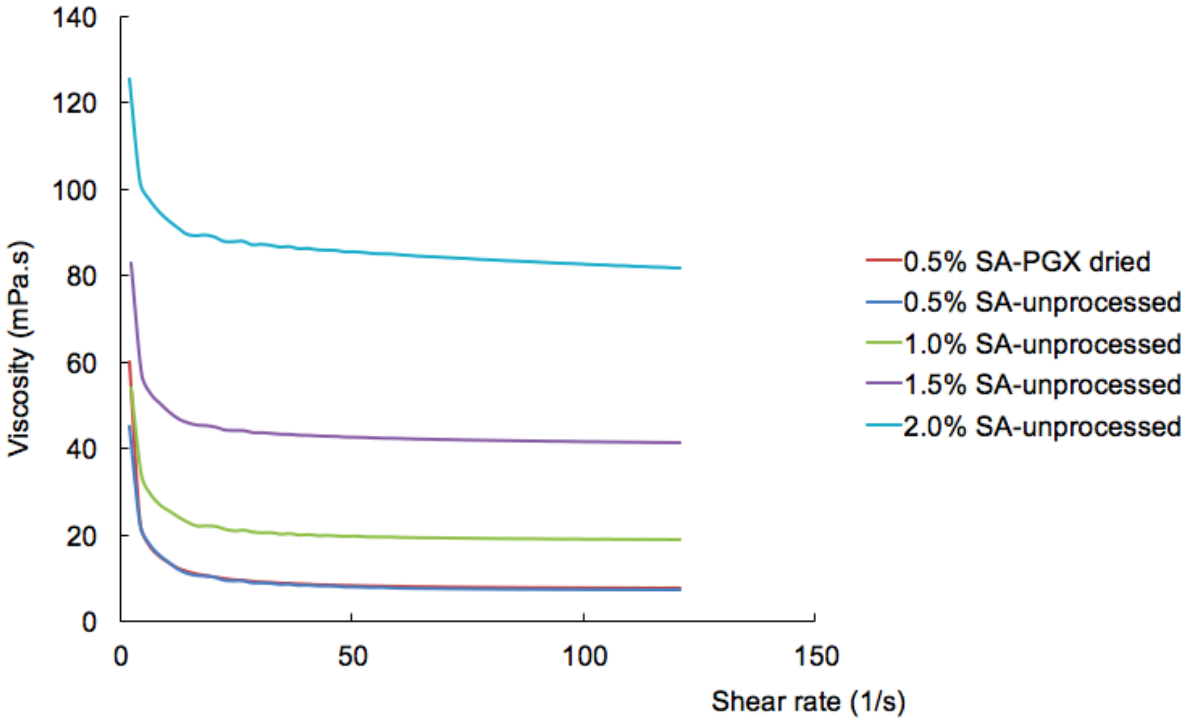

Figure 3.3 Effect of SA concentration on the viscosity of unprocessed SA and PGX-processed SA aqueous solutions (mass flow rate ratio 4:15:5, 15 g/min ethanol flow rate, 1.0% feed conc.) measured at 20 °C.

3.3.2 Morphology

Comparison of the images obtained using HIM as presented in Figure 3.4 showed that the unprocessed SA had large particulates with a smooth surface. After the PGX process, the morphology of the SA changed to a fibrous structure with a fine network of fibrils. Based on Figures 3.5 and 3.6, there were no visible differences between the morphologies of the PGX-dried products after manipulating the processing parameters and the concentration of the aqueous solution. All of the PGX-processed SA samples were composed of a network of

nanofibers, and had similar arrangement and spatial configuration, regardless of the processing conditions applied. The PGX technology was capable of creating a porous structure of SA similar to other water-soluble biopolymers reported previously. Liu et al. (2018) focused on characterizing PGX-dried β-glucan by using HIM, and found that the PGX-processed β-glucan had a highly porous structure as well. However, the alginate material processed by spray drying, resulted in a different morphology compared with the PGX-dried product. Similarly, Tan et al. (2009) obtained a dried product with spherical shape and smooth surface when they used starch and alginate composite to encapsulate ROPUFA, a marine oil, by using spray drying method.

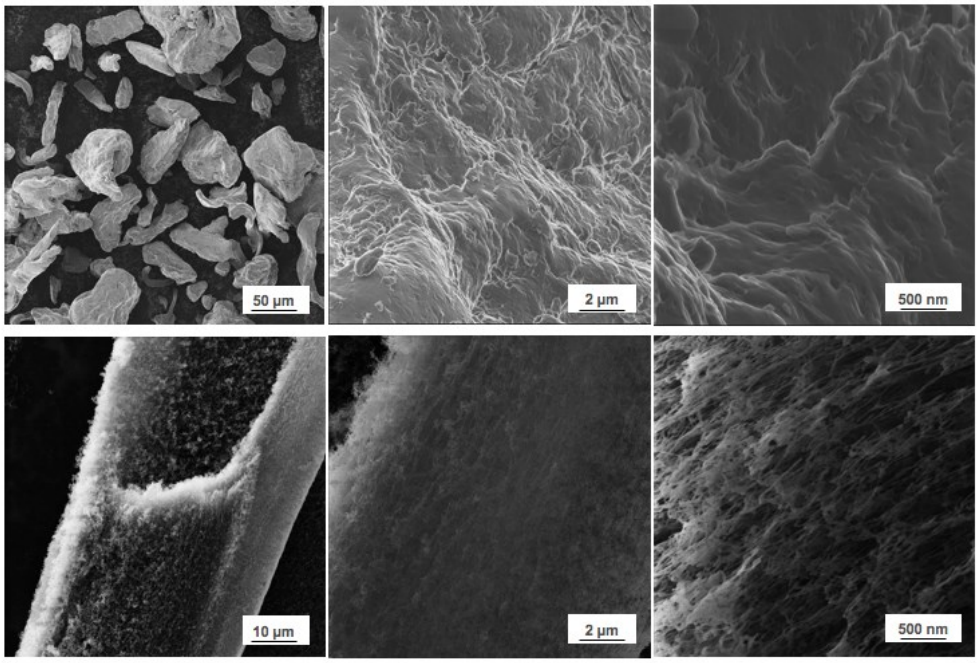

Figure 3.4 HIM images of unprocessed SA (top row), and PGX-processed SA (bottom row) at mass flow rate ratio of 4:15:5, 15 g/min ethanol flow rate, and 1.0% w/w SA solution.

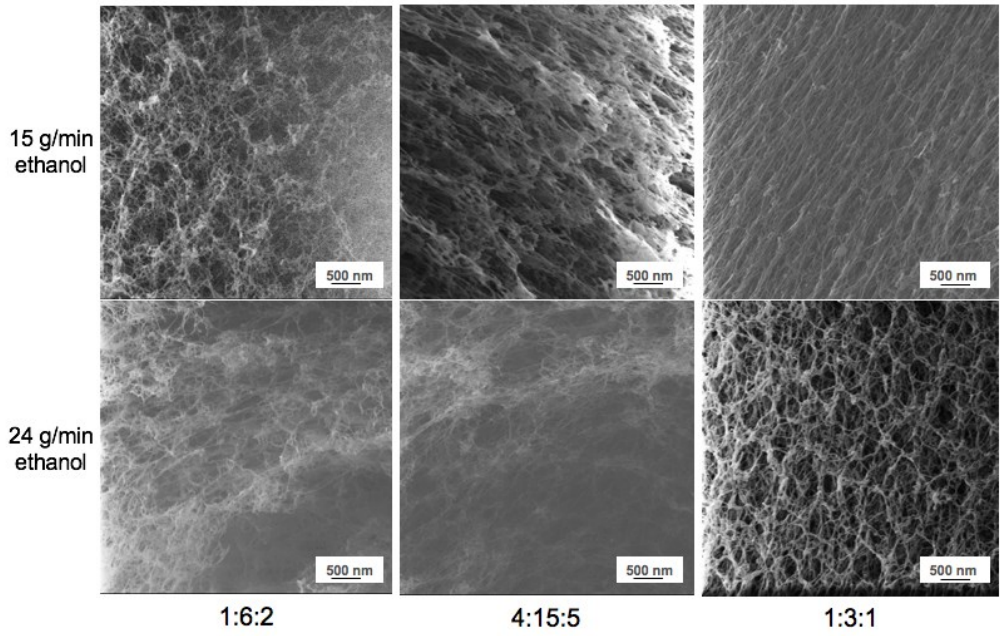

Figure 3.5 HIM images of PGX-processed SA (1.0% w/w). Each row represents different EtOH flow rates, and each column represents different mass flow rate ratios.

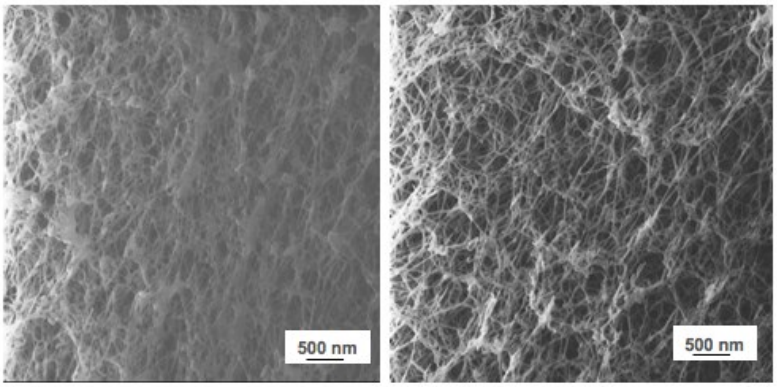

Figure 3.6 PGX-processed SA (mass flow rate ratio 4:15:5, and 15 g/min ethanol flow rate) at different aqueous solution concentrations (left 1.5% w/w, right 2.0% w/w).

3.3.3 Surface area

The specific surface area values were obtained based on the BET method. Figure 3.7 shows that the PGX technology could substantially increase the surface area of the SA compared with the unprocessed sample and the spray dried sample. The dramatic increase in the surface area,

which ranged from 51.3 to 164.5 m^2/g, was due to its porous structure of the fine network of fibrils (Figure 3.4). The conventional drying method, such as spray drying usually results in a low surface area of the dried alginate product. For example, Sun-Waterhouse et al. (2013) focused on microencapsulation of quercetin by SA using spray drying. Based on their BET analysis result, the surface area of 1.31 m^2/g was obtained for the dried product, as compared to 3.5 m^2/g obtained in this study for the spray-dried sample.

Figure 3.8 shows that at a certain mass flow rate ratio, the surface area increased by lowering the flow rate of EtOH. This was because a lower ethanol flow rate could result in a more thorough contact and mixing of the EtOH with the aqueous stream, which then made precipitation and drying of SA more efficient. Moreover, at a certain EtOH flow rate, the mass flow rate ratio of 4:15:5 ($\theta = 5$) resulted in a large surface area (164.5 m^2/g) of the PGX-dried SA. In addition, as shown in Figure 3.9, when SA solutions of different concentrations were processed by using the same processing parameters (mass flow rate ratio of 4:15:5, and the EtOH flow rate of 15 g/min), the surface area of the dried sample increased with decreasing concentration of the aqueous SA solution. This was because the lower concentration SA solution had a much lower viscosity (Figure 3.3), and thus resulted in better mixing with the CO_2 + EtOH mixture at the tip of the co-axial nozzle, and inside of the high-pressure vessel. The SA concentration of 1.0% w/w was chosen as the lowest level to test in this study, because the 0.5% w/w SA solution was very hard to dry, and products with wet spots were usually obtained during the trial runs. In addition, being able to process higher concentrations would be desirable to

increase the throughput of the process.

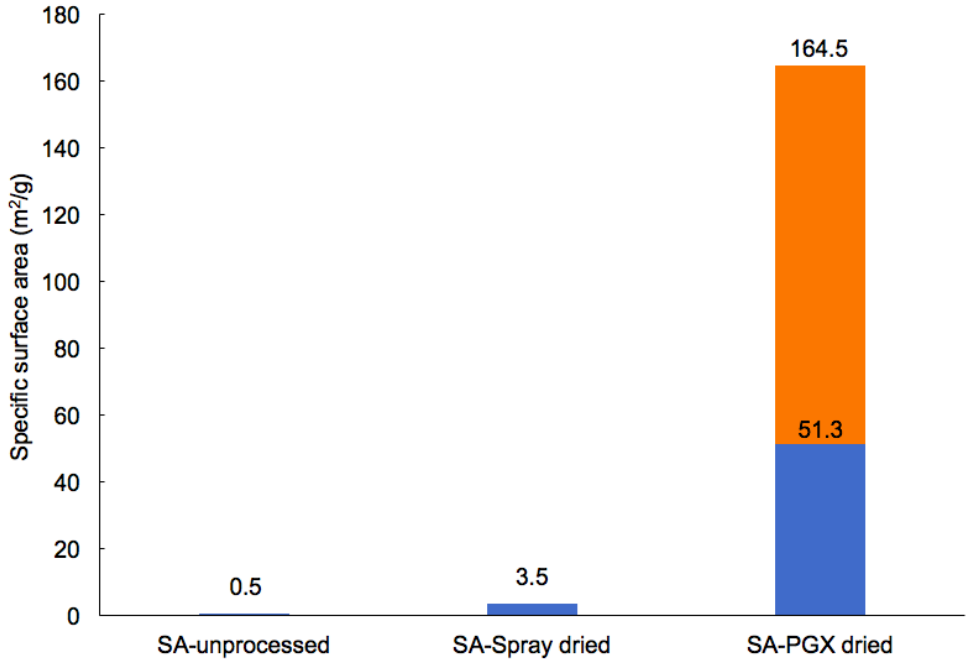

Figure 3.7 Specific surface area of unprocessed SA, 1.0% (w/w) spray dried SA, and the range for 1.0% (w/w) PGX-dried SA obtained at different conditions.

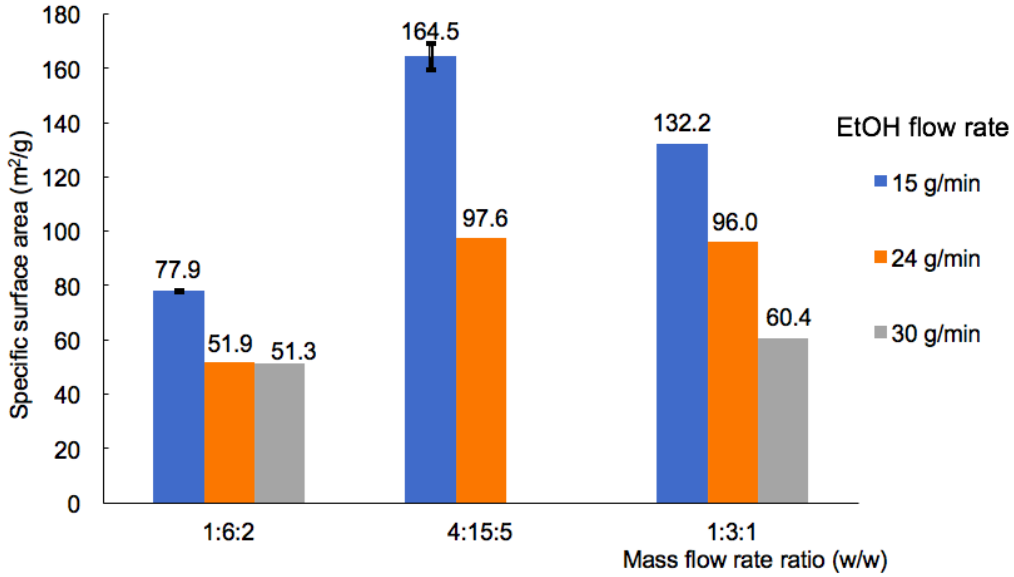

Figure 3.8 Specific surface area of PGX-dried SA (1.0% w/w) obtained at different EtOH flow rates and mass flow rate ratios of SA solution: EtOH: CO_2. Error bars represent mean±standard deviation based on duplicate runs.

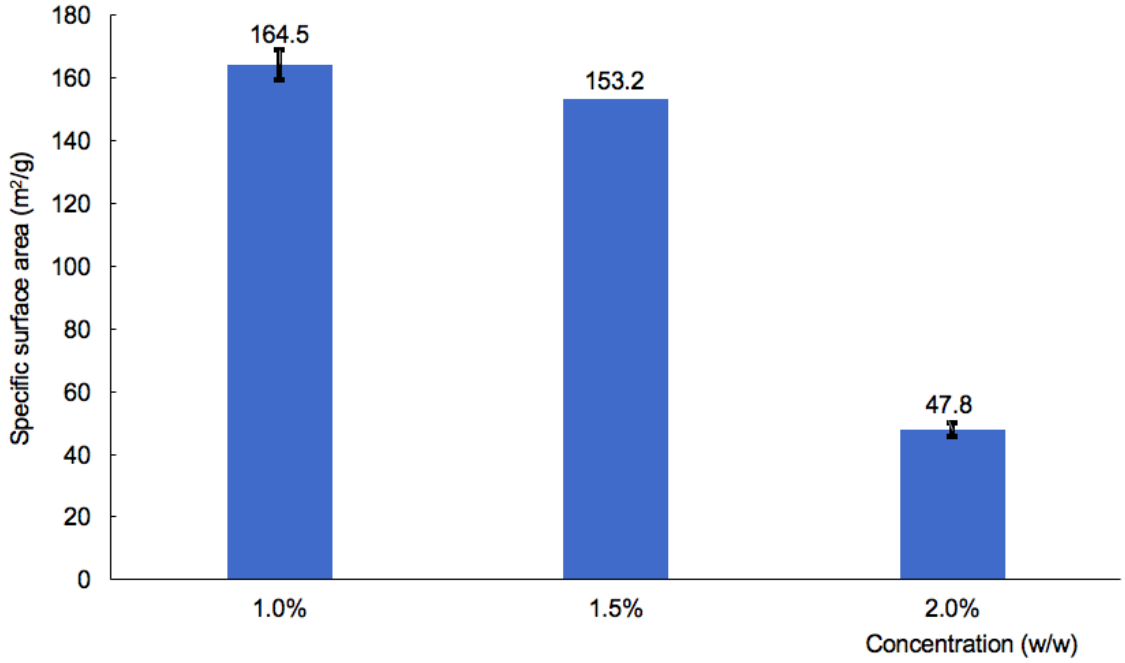

Figure 3.9 Specific surface area of PGX dried SA (mass flow rate ratio 4:15:5, 15 g/min ethanol flow rate) at different SA concentrations of aqueous polymer solution. Error bars represent mean±standard deviation based on duplicate runs.

3.3.4 Differential scanning calorimetry

The DSC results shown in Figure 3.10 indicate that there were no major changes in the thermal behavior of the PGX-processed and unprocessed SA samples, but the exothermic peak, which indicated polymer degradation, shifted to a higher temperature of around 237 °C from 227 °C for the unprocessed sample. The first endothermic peak of the PGX-processed samples was around 60 °C, and that for the unprocessed sample was at 113.8 °C. This may be due to the presence of water in the unprocessed sample, while the PGX-processed sample may have trace amounts of residual EtOH trapped in between the nanofibers. Therefore, the endothermic peak can be due to the evaporation of water, EtOH or both. Sarmento et al. (2006) characterized the

thermal properties of alginate by using DSC, and attributed the formation of the first endothermic peak to water evaporation as well. In addition, they also measured the thermal behavior changes of alginate and chitosan mixture upon a decrease in pH, which was similar to what was happening during the PGX drying process in this study. During the PGX process, temperature and pressure were at 40 °C and 100 bar, respectively, and as CO_2 solubilizes in water, the pH of the system decreases due to the formation of carbonic acid and pH can be around 2.8 (Toews et al., 1995). Moreover, Sarmento et al. (2006) found that a lower pH resulted in a shift of the exothermic peak to a higher temperature, because a lower pH resulted in a more stable complex, and thus a higher amount of energy was required to break the structure. During the PGX process, under high pressure and lower pH due to carbonic acid formation, carboxyl groups on the SA molecule would be neutralized, and thus the repulsion forces between the SA molecules would be less, allowing for more intermolecular interactions. At the end of the process, upon removal of water and release of CO_2, the newly formed interactions between SA molecules might not be reversible, which would explain the shift in the exothermic peak to a higher temperature. Therefore, some alginic acid would be present together with the sodium alginate after the drying process.

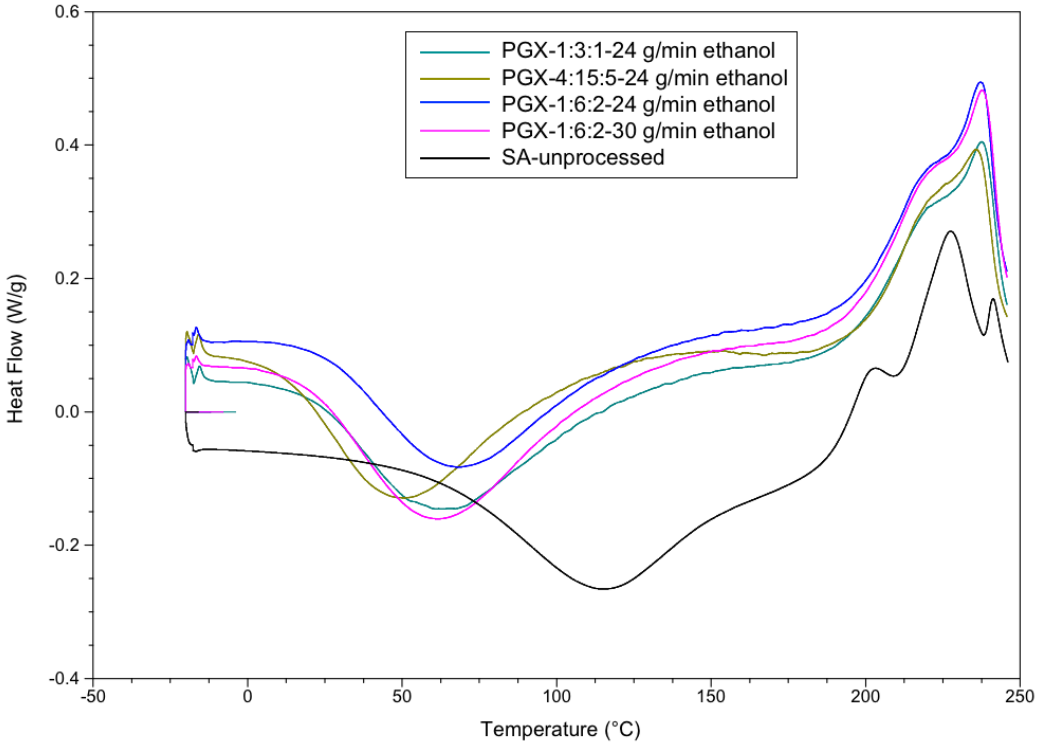

Figure 3.10 DSC thermograms of unprocessed, and PGX-processed SA samples.

3.3.5 Fourier-transform infrared spectroscopy

FTIR analysis was performed to confirm if there was new bond formation or any bond changes occurred after the PGX process. PGX-processed samples obtained under different processing conditions were analyzed by FTIR, and all of them showed approximately identical spectra; therefore, only one typical spectra for the PGX-processed sample was shown in Figure 3.11 to compare with the unprocessed SA. The spectra showed that compared with the unprocessed SA, the PGX-dried SA had a new small absorbance peak at around 1720 cm^{-1}, which indicated carbonyl vibration of the carboxylate group of the SA (Lawrie et al., 2007). This could have happened because during the PGX drying process, the CO_2 dissolves in the water,

resulting in the formation of carbonic acid, leading to the creation of an acidic environment. Therefore, the protonation of the carboxylate group could happen during this process, and form alginic acid. Moreover, the three peaks between 1150 to 1000 cm^{-1} had a stronger absorbance for the PGX-processed samples compared to the unprocessed SA. The first peak in this group of three indicates C—C stretching, the second indicates C—O and C—O—C stretching, and the shoulder of the sharp peak at 1023 cm^{-1} represents strong O—H bending vibration, which could indicate more hydrogen bond formation between the SA molecules after the PGX process (Sartori et al., 1997). Because of the pH decrease followed by the protonation of the carboxylate group, more bond interactions could happen between the functional groups of the SA after the PGX process, which were not present in the unprocessed SA. The spray-dried SA had the highest absorption at almost all characteristic peaks, and was affected the most by the drying process. This might be because it had a higher water content or the molecular interactions were affected by the high processing temperature.

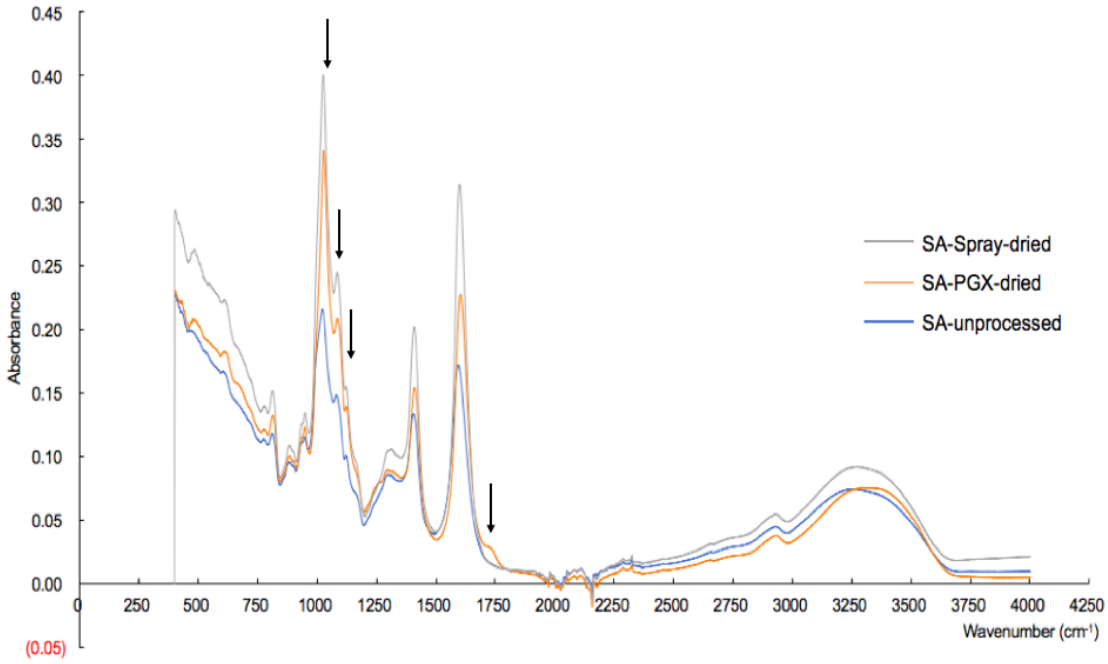

Figure 3.11 FTIR spectra of unprocessed SA, spray dried, and PGX-processed SA

3.3.6 X-ray diffraction analysis

Based on the XRD spectra shown in Figure 3.12, the unprocessed SA has no distinct peaks, which indicate that it is in amorphous form. However, the PGX-processed SA shows a strong peak at around 16°, which indicates that a crystalline or a highly ordered structure was formed after the process. This might have happened during the process, because of the pH shift upon dissolution of CO_2 in water, and allowing the SA polymer chains to interact with each other to form a highly ordered structure. A similar finding was reported by Bhattarai et al. (2006), who were making alginate-based nanofibres by the electrospinning technology. After obtaining the product, XRD analysis was performed in order to compare with the unprocessed alginate powder, and they also found a distinct peak in the alginate nanofibres, which was not present in the

unprocessed sample. They attributed it to the formation of a highly ordered molecular structure.

As a polymer composed of mannuronate and guluronate residues with COO^- at C6 position, it would be expected for SA to be affected by the pH of the medium during processing, whereas that was not the case for β–glucan, which is a neutral polysaccharide of glucose residues (Liu et al., 2018).

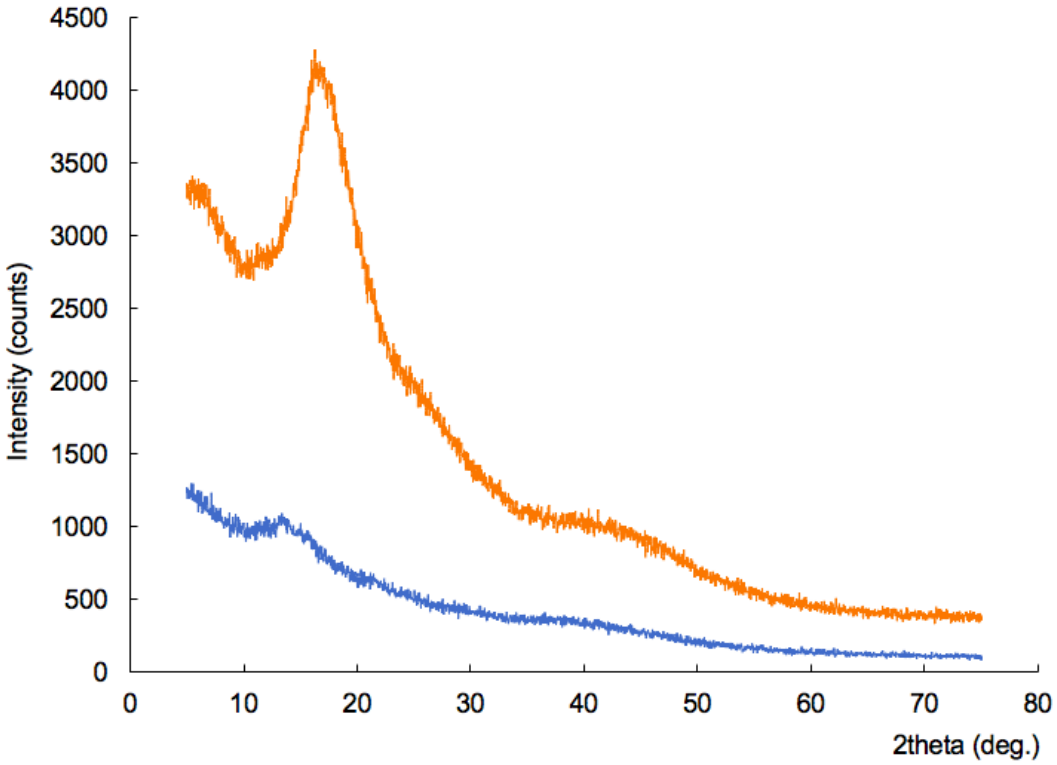

Figure 3.12 XRD analysis of unprocessed (blue color) and PGX-processed (orange color) SA.

3.3.7 Bulk density

The bulk density measurement results (Figure 3.13) show that the PGX-processed SA has a significantly ($p<0.05$) lower bulk density compared with the unprocessed and the spray dried

samples. Since the PGX-dried SA was a porous material, composed of nanofibers (Figure 3.4), it had a very low bulk density, in addition to having a very large surface area (Figure 3.7). Couto et al. (2018b) also measured the bulk density of the PGX-processed β-glucan as 0.006 g/mL, whereas the air-dried β-glucan had a bulk density of around 0.14 to 0.25 g/mL, which decreased more than 23 times after the PGX process. The change in bulk density for SA was more dramatic since the bulk density of the unprocessed sample was 123 times more than that of the PGX-processed sample (0.864 vs. 0.007 g/mL).

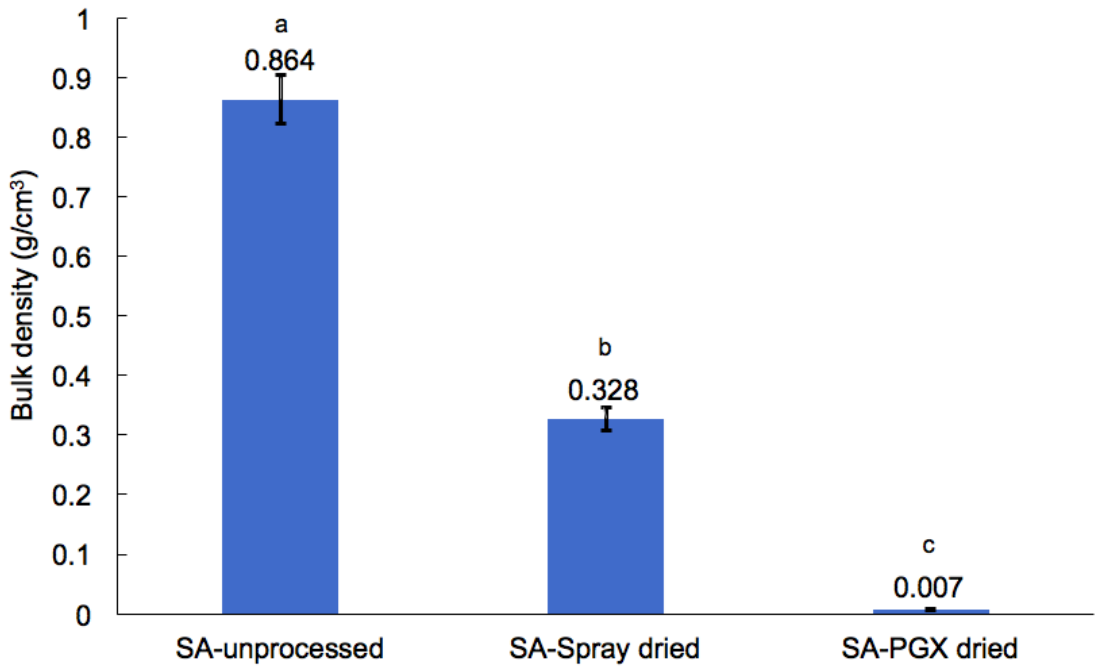

Figure 3.13 Bulk density of unprocessed, spray dried, and PGX-dried SA.
[a-c] Different letters indicate a statistical difference between the mean values ($p < 0.05$). Error bars represent mean±standard deviation based on duplicate runs.

3.4 Conclusions

The PGX drying method is a novel processing technology that can dry the SA efficiently and give it a unique fibrous structure that cannot be obtained by any other drying technology. In this study, the physicochemical properties of the PGX-processed SA obtained at different conditions were determined. The surface area was significantly affected by different processing parameters, and the highest surface area of 164.5 m^2/g was obtained by using the 1.0% w/w SA aqueous solution, 4:15:5 mass flow rate ratio of SA solution:EtOH:CO_2, with the EtOH flow rate of 15 g/min. All PGX-processed SA were composed of nanofibers, with a higher ordered molecular structure and arrangement compared to the unprocessed SA. The thermal behavior was not changed distinctly compared with the unprocessed material. In addition, the bulk density significantly decreased more than 120 times compared with the unprocessed material. The findings of this study would provide more information and expand the application of PGX processing to SA and similar polysaccharides, which would contribute to better understanding and developing the PGX technology in the future.

Chapter 4: Adsorptive precipitation of coenzyme Q10 on sodium alginate dried using Pressurized Gas eXpanded liquid technology

4.1 Introduction

The coenzyme Q10 (CoQ10) is an ubiquinone, which is present in animal and plant cellular membranes and has an essential function during the oxidative phosphorylation process. It is also a lipid-soluble antioxidant that has benefits for human health (Lenaz et al., 1999). Health Canada suggested that less than 300 mg CoQ10 per day would be enough for its antioxidant function, and 30 to 300 mg per day would be beneficial for cardiovascular health (Health Canada, 2007). However, due to the hydrophobic nature of CoQ10, it has limited use in aqueous-based products.

The sodium alginate (SA) is a polysaccharide extracted from brown algae and is composed of (1-4) linked β-D-mannuronate and α-L-guluronate units. The SA is a hydrophilic compound that generally has a molecular weight from 32,000 to 400,000 g/mol (Lee and Mooney, 2012). In addition, because it comes from an abundant marine resource and has unique physicochemical properties, it has broad applications in various products as a nutrient delivery system, gelling agent, stabilizer, and thickener.

The Pressurized Gas eXpanded (PGX) liquid technology invented by Temelli and Seifried (2016) is based on the anti-solvent method that is able to dry high molecular weight biopolymers from aqueous solution and results in unique morphologies, which is not possible to achieve by other conventional drying methods. In this study, the PGX-processed SA (PGX-SA) was used as the carrier for CoQ10. The PGX-SA has a very large surface area (as high as 164.5 m^2/g) as

reported in Chapter 3, compared with the commercially available SA (0.5 m^2/g); therefore, it has great potential as a delivery system to be loaded with a large amount of CoQ10, which can then be used in aqueous-based products for CoQ10 fortification.

Supercritical carbon dioxide (SC-CO_2) can be used for delivering bioactive compounds into biopolymers without using organic solvents. For example, SC-CO_2 can be applied to solubilize the hydrophobic bioactive material, and then be used as a carrier to load the bioactive compound onto the biopolymer. Firstly, the pressure of the system is manipulated to a certain value, considering equipment limitations, in order to solubilize the highest amount of bioactive in the SC-CO_2 stream. Then, as the SC-CO_2 stream is contacted with the biopolymer, some of the bioactive would be adsorbed onto the surface of the biopolymer based on their affinities. Finally, during depressurization, the bioactive compound present in the SC-CO_2 stream is precipitated onto the biopolymer. This whole process is referred to as adsorptive precipitation and the mechanism of this process was recently reviewed by Gurikov and Smirnova (2018).

The adsorptive precipitation process has been applied to make drug delivery systems, for example, loading ketoprofen on starch-based aerogels, and loading benzoic acid on silica aerogels (Gorle et al., 2010; García-González and Smirnova, 2013). However, there is lack of information on the use of this process for CoQ10 delivery, targeting applications in food or cosmetic products. Therefore, the objective of this study was to investigate the effect of different processing parameters (circulation time and rate, operation pressure, and form of biopolymer) on the CoQ10 loading on PGX-SA during the adsorptive precipitation process, and to characterize

the physicochemical properties (CoQ10 loading content, particle morphology, thermal behavior, molecular-level structure, and dispersion in an aqueous system) of the loaded samples.

4.2 Materials and methods

4.2.1 Materials

Alginic acid sodium salt powder extracted from brown algae was purchased from Sigma-Aldrich (product No. 180947, Oakville, ON, Canada). PGX-SA for the adsorptive precipitation experiments was supplied by Ceapro Inc. (March 1, 2019 batch, obtained at 100 bar, 40 ºC, 1.0% w/w aqueous SA solution, and flow rates of 40 g/min SA solution, 150 g/min ethanol, and 50 g/min CO_2). CoQ10 (98.34% purity) was obtained from PureBulk (Roseburg, OR, USA) and CO_2 (99.9% purity, < 3 ppm H_2O) was purchased from Praxair Canada Inc. (Mississauga, ON, Canada).

4.2.2 Adsorptive precipitation unit

The adsorptive precipitation unit described previously by Couto et al. (2018b) was modified and simplified to accommodate the single step recirculation operation to meet the objectives of this study. The flow diagram of the unit was presented in Figure 4.1 and it was composed of two high-pressure vessels containing PGX-SA (biopolymer vessel, 42.5 mL volume) and CoQ10 (bioactive vessel, 6.2 mL volume). The modified adsorptive precipitation unit had a total internal volume of 190 mL, which was determined by first pressurizing the whole system to 300 bar using CO_2, and then slowly depressurizing the system, while the volume of CO_2 leaving the

system was measured with a flow meter (Canadian Meter Company Limited, Type AL225, Cambridge, ON, Canada) connected to the exit. Then the volume of CO_2 measured at ambient conditions was converted to the volume of the system by multiplying it with the ratio of densities of CO_2 at atmospheric pressure to that at 300 bar). These two vessels were placed inside an oven (Fisher, Econotemp 15F, Pittsburg, PA, USA) to control the temperature. The unit was pressurized by a syringe pump (Teledyne ISCO, model 260D, Lincoln, NE, USA) at a CO_2 flow rate of 8 mL/min (measured at -15 ºC of the pump head), and a magnetic drive gear pump (Micropump, GAH−T23.J9FS.Z−N1CH50, Vancouver, WA, USA) was used to recirculate the CO_2 inside the system. A slow initial pressurization rate was applied to minimize compaction of the bed of PGX-SA powder and maintain it in the form that was initially placed into the biopolymer vessel. A micrometering valve (V8) (Parker Autoclave Engineers, 10VRMM2812, Erie, PA, USA) was placed at the end of the unit for manually controlling the depressurization rate of the system.

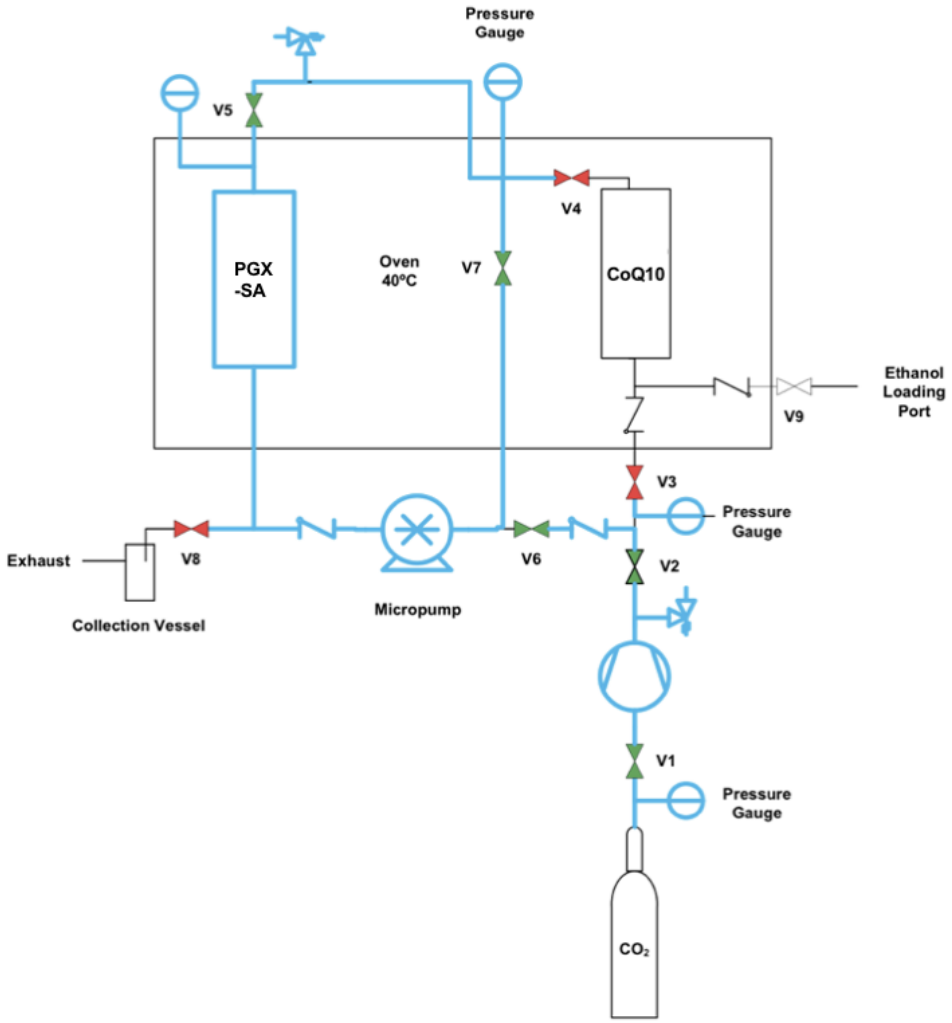

Figure 4.1 Flow chart of the adsorptive precipitation unit.

For each adsorptive precipitation run, 0.3 g PGX-SA was loosely packed and placed inside a glass tube, so that the dimension of the packed bed of biopolymer was always around 12 cm high * 1.1 cm diameter. The glass tube with the biopolymer was then put inside of the biopolymer vessel with felt filters (polyester felt, pore size 5 μm, McMaster-Carr, Aurora, OH, USA) on both ends. Moreover, 0.5 g of CoQ10 was placed inside the bioactive vessel with felt filters on both ends as well. After the temperature was stabilized at 40 ºC, the bioactive vessel, which contained

the CoQ10 was isolated by closing the valves at its inlet and exit (V3 and V4), and then CO_2 was introduced to pressurize the rest of the unit by the syringe pump. After the pressure reached the target value, the micropump was started to recirculate the CO_2 inside the system for achieving thermal equilibrium. Then, the valves for isolating the bioactive vessel were opened, V7 was closed and the unit was repressurized to the targeted pressure. The recirculation speed of the micropump could be adjusted for manipulating the flow rate of the CO_2 + CoQ10 stream to pass through the PGX-SA bed. After a desired adsorption time, the micropump was turned off, and then the biopolymer vessel was isolated (V5 and V6 closed) and fast depressurized at 3.33 bar/sec through the micrometering valve. During the depressurization step, the CoQ10 solubilized in SC-CO_2 would precipitate onto the PGX-SA bed to finish the process.

4.2.3 Experimental design

Three different parameters were tested in this study, as shown in Table 4.1, which included the combination of circulation time and rate (25 min X 190 mL/min, 50 min X 130 mL/min, 40 min X 262 mL/min, and 50 min X 262 mL/min), operation pressure (200, 250, and 300 bar), and the form of PGX-SA (original form and ground form). Three sets of experiments were performed, testing the three variables investigated one variable at a time while keeping the other two constant. The ‘original form’ of the PGX-SA refers to directly putting the sample from Ceapro Inc. into the biopolymer vessel, while the ‘ground form’ refers to manually grinding the PGX-SA by using a herb grinder first, and then putting it into the biopolymer vessel. The original form of PGX-SA had a long-fibrous structure; however, after it was ground into smaller particles, it

would have a larger surface area. Thus, after comparing the CoQ10-loaded product properties, the effect of different biopolymer forms and surface areas on this process could be evaluated. The combination of circulation time and rate was related to the amount of CO_2 (or the amount of CoQ10 solubilized in SC-CO_2) that passed through the biopolymer vessel, which was directly related to the adsorption step. The circulation rate was measured at ambient conditions using ethanol, and then converted to the circulation rate of CO_2 under each condition based on the density difference between them (Couto et al., 2018b). In addition, a depressurization rate of 3.33 bar/sec was employed in all the runs, and all experiments were performed in duplicate.

Table 4.1 Experimental conditions tested for adsorptive precipitation of CoQ10 on PGX-SA

Experiment	Circulation time (min)	Circulation rate (mL/min)	Operation pressure (bar)	Form of biopolymer
1	25	190	300	Original
2	40	262	300	Original
3	50	130	300	Original
4	50	262	300	Original
5	40	262	250	Original
6	40	262	200	Original
7	40	262	300	Ground

4.2.4 Characterization of loaded products

4.2.4.1 CoQ10 loading content

The amount of CoQ10 in the loaded PGX-SA particles was determined by using the UV

spectrophotometer (FLAME-S-XR1-ES Assembly from 200-1050 nm, Ocean Optics, Dunedin, FL, USA) at the wavelength of 270 nm. Firstly, 20 mg CoQ10-loaded SA (L-SA) was mixed with 20 mL hexane to dissolve the CoQ10, the L-SA was soaked at ambient temperature for 1.5 h (mixed manually every 30 min) and covered with aluminum foil to prevent light degradation of the CoQ10. During the CoQ10 extraction period, PGX-SA precipitated to the bottom of the glass vial quickly giving a clear supernatant, and the 10× dilution of the supernatant was prepared for the UV measurement. Moreover, a 10-point (0.01 - 0.10 mg/mL) standard curve was established by using pure CoQ10 in hexane, in order to determine the loading amount of the L-SA. The standard solution was prepared by mixing 20 mg CoQ10 with 20 mL hexane, and diluting 10× to make the 0.10 mg/mL CoQ10 in hexane solution. Then, this standard solution was further diluted accordingly to prepare the 10-point standard curve. The measurements were done in triplicate, and the R^2 value of the standard curve was 0.998. The CoQ10 loading percentage was calculated by using Eq. (4.1):

$$CoQ10\ loading\% = (W_{CoQ10\ loaded} / W_{L\text{-}SA}) \times 100 \qquad (4.1)$$

4.2.4.2 Particle morphology

The morphology of PGX-SA, L-SA, and a 30% (w/w) physical mixture (PM) of CoQ10 and PGX-SA were examined by using Zeiss Orion Helium Ion Microscope (Ostalbkreis, BW, Germany), which was located at NanoFab, University of Alberta, as described in Chapter 3 (Section 3.2.4.2).

4.2.4.3 Differential scanning calorimetry analysis

Thermal behavior of PGX-SA, L-SA, and PM were determined by using a DSC Q2000 system (TA Instruments, Mississauga, ON, Canada) calibrated with indium standards. Approximately 4 to 6 mg sample was placed into an aluminum pan for each measurement, and an empty pan was used as the blank. Measurements were carried out at the heating rate of 5 °C/min from 0 to 250 °C, with a modulation of +/- 1.00 °C every 60 sec. Data were interpreted by using Advantage software.

4.2.4.4 Fourier-transform infrared (FTIR) spectroscopy analysis

FTIR measurement was performed by using iS50 FTIR Spectrometer (ThermoFisher Scientific, Waltham, MA, USA) as described in Chapter 3 (Section 3.2.4.5).

4.2.4.5 X-ray diffraction analysis

PGX-SA, CoQ10, L-SA, and PM were examined by using Bruker D8 Discover diffraction system (Bruker, Billerica, MA, USA), equipped with Cu-source and high throughput LynxEYE 1-dimentional detector as described in Chapter 3 (Section 3.2.4.6).

4.2.4.6 Dispersion in aqueous system and storage stability test

The aqueous dispersions of PGX-SA, L-SA, and PM were prepared by re-dispersing 10 mg samples in 10 mL de-ionized water, and stored in the dark environment at 4 °C for 50 days for the storage stability test.

4.2.4.7 Zeta potential of dispersion in aqueous system

Zeta potential of PGX-SA, L-SA, and PM was measured by re-dispersing 10 mg samples in

10 mL de-ionized water, followed by a 10x dilution, and using Zeta-sizer (Nano ZS Malvern Instruments, Malvern Panalytical Ltd., Malvern, UK). The measurement was performed at 25 °C, with at least 10 runs for each sample, and the mean value is reported.

4.2.4.8 Statistical analysis

Statistical analysis was performed using RStudio 1.1.383 (R Core Team, 2015). One-way analysis of variance (ANOVA) was performed for CoQ10 loading content, and means were compared by using paired t-test of least square means with significance difference defined at $p < 0.05$.

4.3 Results and discussion

4.3.1 CoQ10 loading

The CoQ10 loading content obtained at each processing condition tested was shown in Figure 4.2. In the first set of experiments, keeping pressure constant at 300 bar and using the original PGX-SA as the biopolymer, the CoQ10 loading increased significantly ($p<0.05$) as the circulation time and circulation rate was increased during the adsorptive precipitation process. High circulation time and rate contributed to more even and thorough CoQ10 contact with the biopolymer, and then resulted in a higher loading on the surface of PGX-SA. Couto et al. (2018b) focused on adsorptive precipitation of CoQ10 on PGX-processed β-glucan. They also found that the loading amount increased with increasing circulation time and rate, but only up to a certain point, since the loading decreased after a long circulation time, because the CoQ10 was then

washed away by the SC-CO_2.

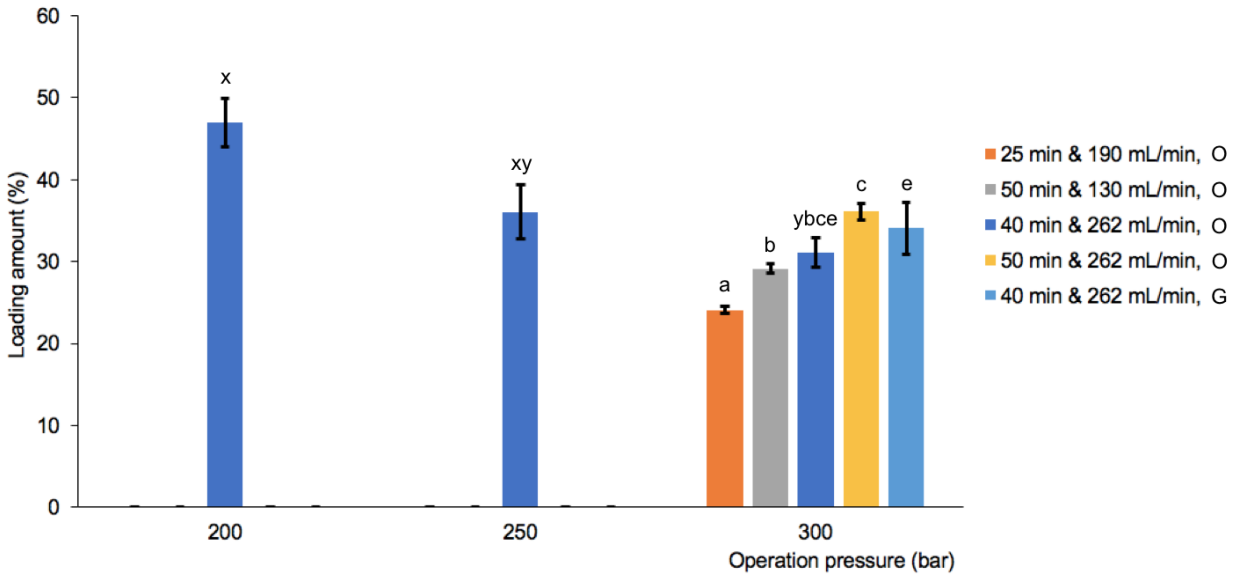

Figure 4.2 CoQ10 loading obtained at different processing conditions. O (original form of the PGX-SA), G (ground form of the PGX-SA).

[x-y] Different letters for each operation pressure (40 min & 262 mL/min circulation condition, and biopolymer in original from) indicate a significant difference between the mean values ($p < 0.05$).

[a-c] Different letters for operation pressure at 300 bar (biopolymer in original form) indicate a significant difference between the mean values ($p < 0.05$).

[e-f] Different letters for original and ground samples (operation pressure at 300 bar, 40 min & 262 mL/min circulation condition), indicate a statistical difference between the mean values ($p < 0.05$).

In the second set of experiments, the circulation time and rate were kept constant using the original PGX-SA as the biopolymer, but the operation pressure was varied. The CoQ10 loading amount increased significantly ($p<0.05$) with a decrease in pressure. This can be explained by considering the amount of CoQ10 solubilized in SC-CO_2 in the system at different pressures. The

total internal volume of the system was 190 mL (as mentioned in Section 4.2.2). According to Matias et al. (2004), the solubility of CoQ10 in SC-CO_2 at 40 °C and 211 bar was $6.62x10^{-5}$ mole fraction. Therefore, the SC-CO_2 in the system could solubilize approximately 0.207 g of CoQ10 at 200 bar, and after some of the CoQ10 was adsorbed onto the PGX-SA, the SC-CO_2 could solubilize more CoQ10 and load it onto the PGX-SA since 0.5 g of CoQ10 was placed in the vessel at the beginning of each experiment. In terms of the available solubility data, Matias et al. (2004) measured the CoQ10 solubility in SC-CO_2 by using a static system. However, Couto et al. (2018a) used a dynamic system to measure CoQ10 solubility in SC-CO_2, and based on their result, the amount of CoQ10 that could be solubilized at 200 bar in this setup would be 0.019 g (calculated based on the linear regression between the density of SC-CO_2 and the solubility of CoQ10 at 40 °C: $\ln S = 11.807 * \ln \rho - 81.814$), which was nearly 10 times less compared with the values reported by Matias et al. (2004). Even though the setup used in this study was a dynamic loading system, the results seemed to fit better, considering the solubility data of Matias et al. (2004). After the circulation period, all CoQ10 placed in the bioactive vessel was solubilized into the SC-CO_2, and there was no CoQ10 residue left after opening the bioactive vessel. The amount of CoQ10 (0.5 g) placed in the bioactive vessel was kept constant throughout all processing conditions in this study. The solubility of CoQ10 in SC-CO_2 increases with pressure and reaches $11.29x10^{-5}$ mole fraction at 262 bar (Matias et al., 2004) and therefore, saturation of SC-CO_2 in the system was probably not reached at 300 bar. Then, the SC-CO_2 could have the potential to wash away some of the CoQ10 from the PGX-SA, which could be

one of the reasons why the loading was higher at 200 bar. Moreover, because the CO_2 has lower density and thus lower solvent power at low pressures, the affinity between PGX-SA and CoQ10 would be higher. A similar result was obtained by Kjellow et al. (2010), who investigated the partitioning of three kinds of biocides between SC-CO_2 and wood at different pressures and temperatures. They found that when CO_2 density was lower, the affinity of all three kinds of biocides to the wood was higher. In addition, during the depressurization step, it would take a shorter time for the CoQ10 to precipitate out of the CO_2 stream at the lower operation pressure, which also contributed to the higher loading amount.

In the third set of experiments, the original or ground form of PGX-SA was used at fixed conditions of circulation time and rate and operation pressure (300 bar). It was expected that grinding the PGX-SA would result in a higher loading amount compared to its original form. The increased surface area of the ground sample (from 62.5 m^2/g to 109.45 m^2/g) made it possible to load slightly more CoQ10, but there was no significant difference ($p>0.05$) between the ground and original biopolymer for their CoQ10 loading content.

The processing condition to obtain the highest CoQ10 loading content (46.9% w/w) was at 200 bar, with 40 min and 262 mL/min circulation time and rate, and by using the PGX-SA in original form. The one factor at a time approach used in this study did not allow the assessment of interaction effects and further research is needed to evaluate the interaction effects between the parameters tested. The CoQ10 loading content can also be interpreted by considering the amount of CoQ10 loaded on each square meter of the surface of PGX-SA. In this case, under the

best processing condition, 7.51 mg CoQ10/m^2 PGX-SA could be loaded, which was similar to the highest loading result (7.2 mg/m^2) obtained by Couto et al. (2018b) for β-glucan. This could be because these two linear polysaccharides were able to form similar interactions with the CoQ10 molecule during the adsorptive precipitation process despite the fact that SA was a charged polymer while β-glucan was natural. Couto et al. (2018b) also performed adsorptive precipitation of CoQ10 on stainless steel frits, in order to identify if there were interactions between CoQ10 and PGX-processed β-glucan or it was only physical deposition. The CoQ10 loading on stainless steel frits was only 3.2 mg/m^2, which proved that there were molecular interactions between CoQ10 and β-glucan. Similarly, the loading of 7.51 mg/m^2 on PGX-SA obtained in this study indicates the level of interaction between CoQ10 and PGX-SA.

4.3.2 Morphology

Particle morphology was assessed using HIM. There was no major difference between the morphology of the loaded samples (all samples were analyzed and a typical image was presented in Figure 4.3), regardless of the different parameters applied in terms of operation pressure, circulation time and rate, or grinding the biopolymer. Compared with the PGX-SA, the L-SA had thicker fibers, which were covered by CoQ10. In addition, Figure 4.3 shows that the CoQ10 was homogeneously distributed on the surface of the biopolymer. Moreover, the image of the PM showed that the CoQ10 aggregates were just present on the surface of the biopolymer, which were not evenly distributed on the surface. Liu et al. (2018) also characterized CoQ10-loaded PGX-processed β-glucan by using HIM, and found that the CoQ10 was evenly dispersed on the

surface of the β-glucan in the form of spherical particles, with a diameter from 35 to 160 nm. Compared with the L-SA (31.14% w/w) used for the HIM analysis in this study, their CoQ10 loading amount was very low (1.4% w/w), which was probably not sufficient to cover the surface. It is apparent that different processing conditions, as well as the different properties of the biopolymers, could result in different morphologies.

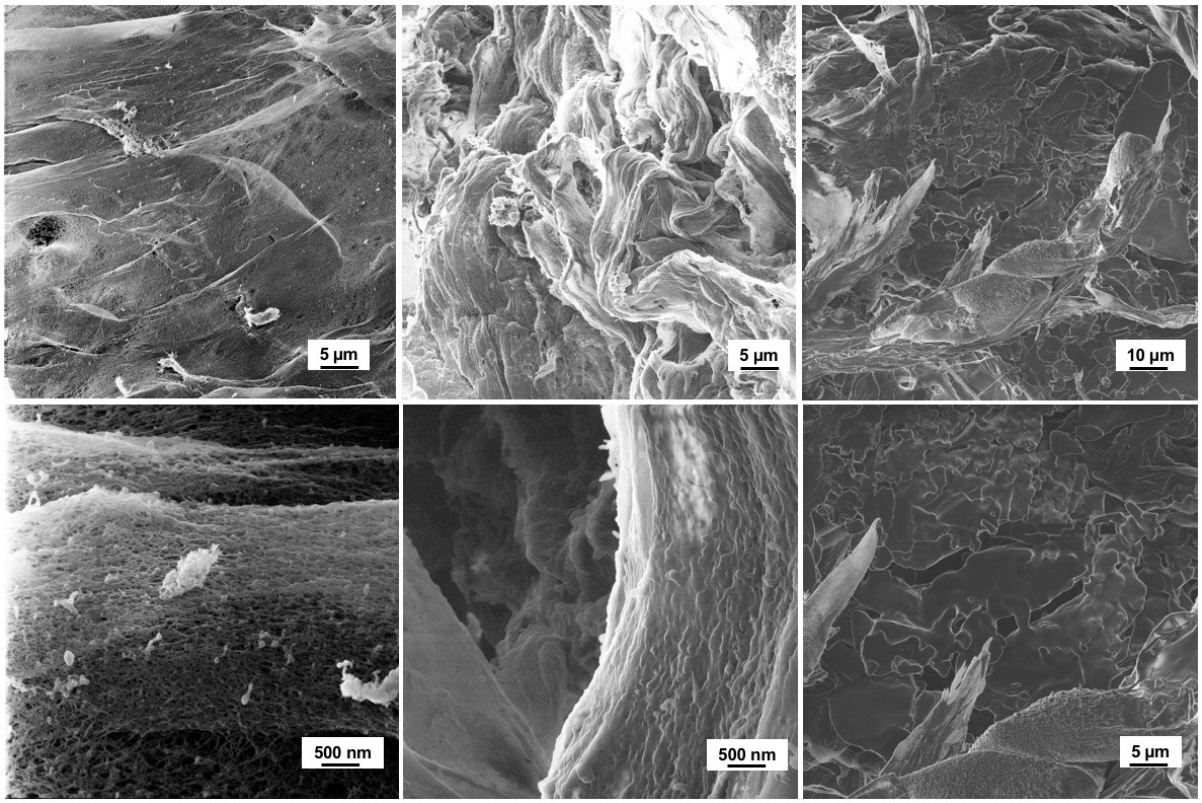

PGX-SA L-SA PM

Figure 4.3 HIM images of PGX-SA, L-SA (processed at 300 bar, 40 min & 262 mL/min, original form), and 30% PM of CoQ10 and PGX-SA.

4.3.3 Fourier-transform infrared spectroscopy

FTIR analysis was performed to examine the interactions between the biopolymer and

CoQ10. There was no difference between the different loaded samples obtained at different operation pressures, circulation times and rates, or grinding the biopolymer. Comparison of the FTIR spectra of PM and the L-SA presented in Figure 4.4 showed that there was no new peak or major intensity difference between the two spectra, indicating that there was no new covalent bond formation between the CoQ10 and biopolymer after this process. Moreover, Figure 4.5 shows the FTIR spectra for L-SA and CoQ10, demonstrating that some characteristic peaks of the CoQ10 were also present in the L-SA spectra. For example, the peak at 1645 cm^{-1} could be associated with the C=O stretching, and the peak at 1609 cm^{-1} could be correlated with the C=C stretching in the ring (Stuart, 2004). In addition, peaks at 1270, 1262 and 1204 cm^{-1} could be related with the C-O stretching from the CH_3O group, and peaks at 1445 and 1383 cm^{-1} could indicate the C-H bending from methyl group (Stuart, 2004). The peak around 3300 cm^{-1} for the PM was more intense than that for the L-SA, which indicated that there was more O-H stretching vibration in the PM (Stuart, 2004). This indicated that the surface of L-SA was more homogeneously covered with CoQ10, and thus the O-H stretching from the PGX-SA was masked and less obvious than that in the PM. The two FTIR spectra indicated that there was no obvious new covalent bond formation, and the loaded CoQ10 still displayed most of its characteristic peaks after the adsorptive precipitation process. Some small peaks of the CoQ10 were covered by the broad peak of L-SA, which might have hidden some characteristic peaks formed between the PGX-SA and CoQ10. Similar results were also shown by Couto et al. (2018b), where the characteristic peaks of CoQ10 were present after loading it onto β-glucan and

no new covalent bond formation was apparent after the adsorptive precipitation process.

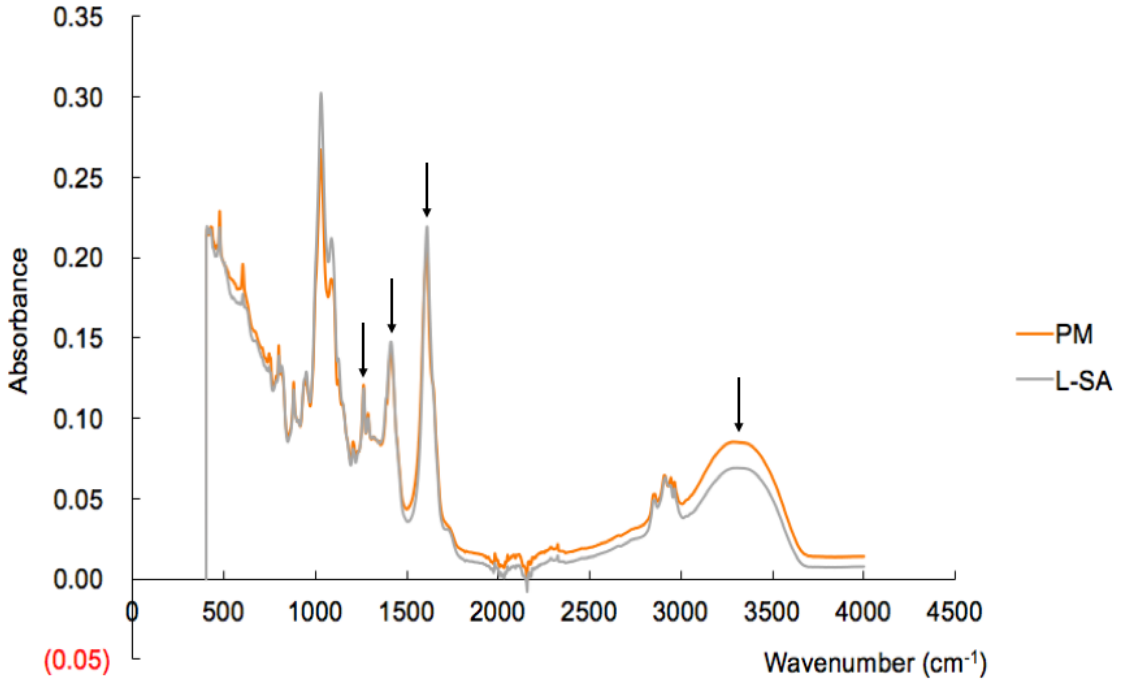

Figure 4.4 FTIR spectra for PM and L-SA.

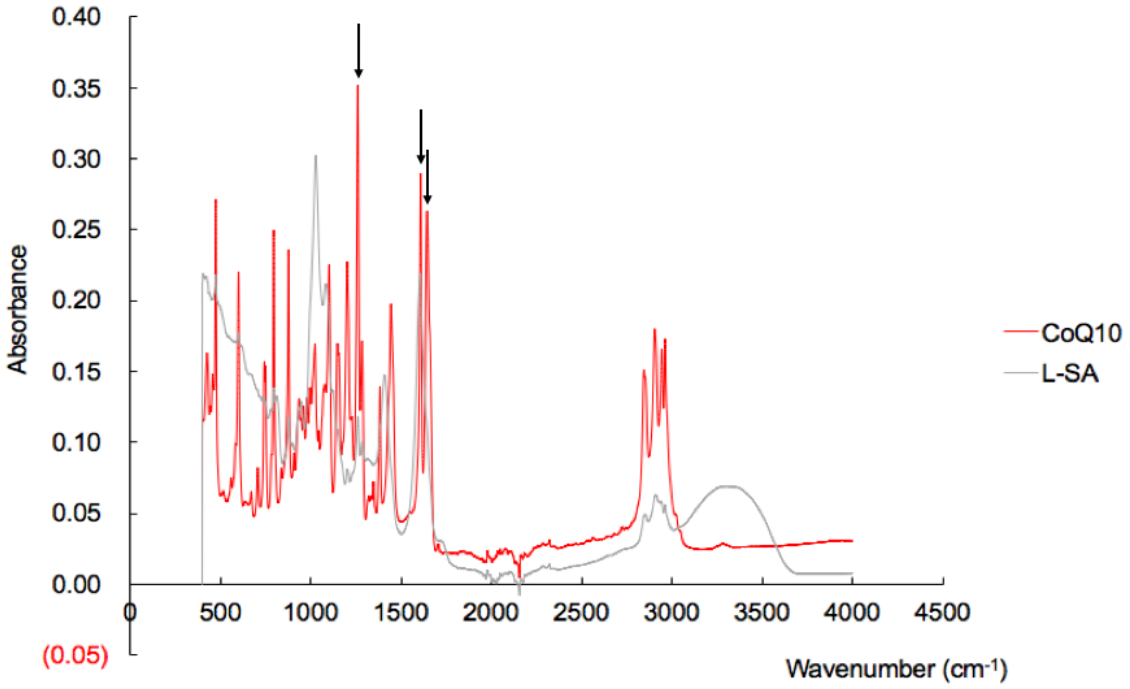

Figure 4.5 FTIR spectra for CoQ10 and L-SA.

4.3.4 Differential scanning calorimetry

The DSC analysis results were shown in Figure 4.6. The PM had the same onset, offset and endothermic peak as the pure CoQ10, which indicated that there were no chemical interactions between these two compounds upon only physically mixing them. However, both L-SA samples showed an endothermic peak shifting to a lower temperature, and a wider width between the onset and offset points compared with the PM or CoQ10. This shifting of the crystallization temperature of the CoQ10 in the L-SA might be affected by the thermal history, or the interaction between SC-CO_2, PGX-SA, and the CoQ10 during the adsorptive precipitation process. Moreover, the DSC result together with the XRD results presented in the next section indicated that the CoQ10 was still in the crystalline form after the adsorptive precipitation process. Kwon et al. (2002) used DSC to characterize the thermal behavior of CoQ10-loaded poly-(methyl methacrylate). They also found a shift in the endothermic peak of CoQ10 to a lower temperature after the loading process, which was explained by the new interactions formed between the polymer and CoQ10 after the loading process, followed by rearrangement of the CoQ10 in the polymer network, hindering the crystal behavior of the bioactive compound. Hsu et al. (2003) prepared CoQ10 nanoparticles with emulsifying wax; their DSC results showed no shifting of the endothermic peak of the physical mixture, but a shift was observed for the prepared CoQ10 nanoparticles. They explained that there might be interactions between the wax and CoQ10, which resulted in the endothermic peak shifting to a lower temperature.

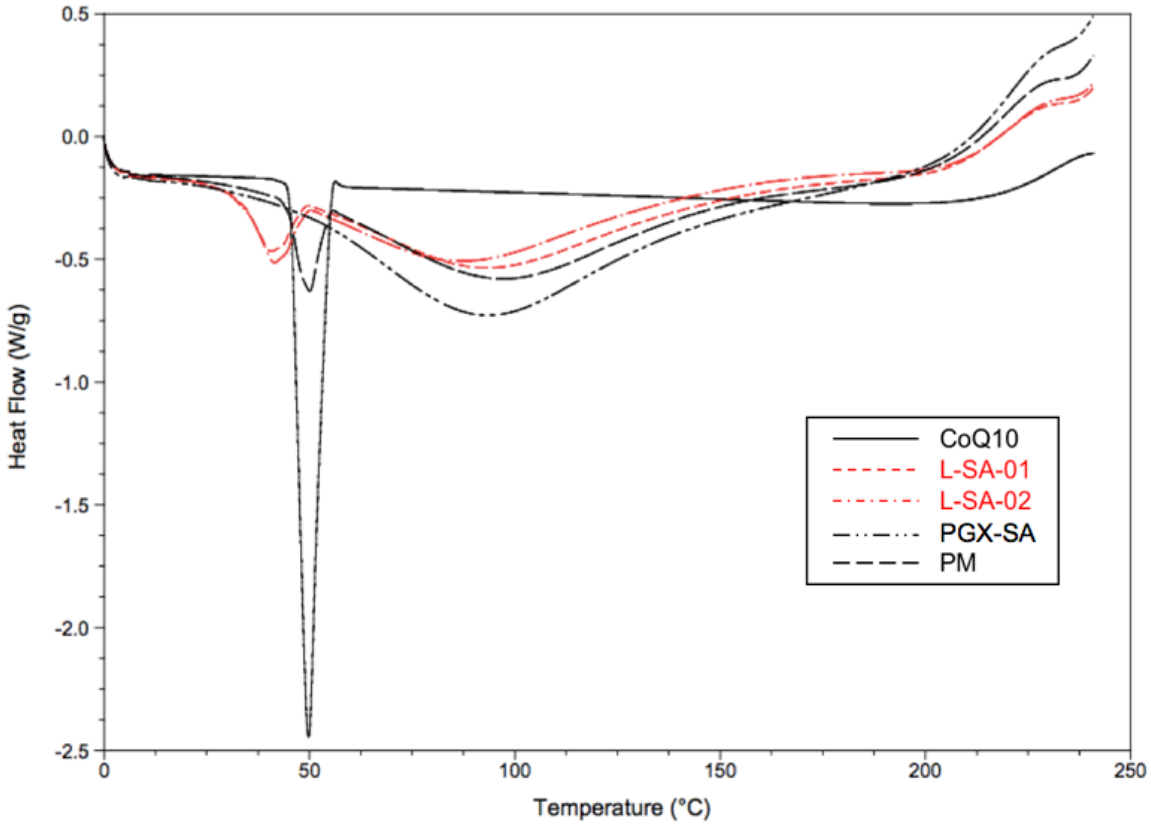

Figure 4.6 DSC analysis results (L-SA-01 was processed at 300 bar, with 40 min & 262 mL/min, and biopolymer in original form; L-SA-02 was processed at the same conditions using biopolymer in ground form).

4.3.5 X-ray diffraction analysis

From the XRD analysis results shown in Figure 4.7, the characteristic peaks of CoQ10 were also present in both CoQ10-loaded SA and the physical mixture. This indicated that the CoQ10 loaded on the SA was still in its crystalline form rather than the amorphous form, even after being solubilized into and precipitated out of the SC-CO_2. Liu et al. (2018) characterized the CoQ10-loaded PGX-processed oat β-glucan using XRD to examine the crystallinity of CoQ10. Initially, they found that the CoQ10 was in its amorphous form after the loading process, but it

was also possible that the CoQ10 peak could be hidden under the broad peak of β-glucan because of the low loading amount (1.4% w/w) of CoQ10. Indeed, after hydrolyzing the β-glucan, they found that a small portion of CoQ10 was still in the crystalline form in their loaded sample. However, the L-SA used for XRD analysis in this study contained 31.14% (w/w) CoQ10, which was more than 20 times compared with the CoQ10-loaded β-glucan analyzed by Liu et al. (2018). Therefore, the characteristic peaks were more clear and evident. On the other hand, the amorphous form of CoQ10 has a faster dissolution rate and a higher bioavailability compared to its crystalline form (Yu, 2001). Therefore, it is desirable to have CoQ10 in its amorphous form and further research is needed to decrease the extent of crystallinity of CoQ10 in the L-SA.

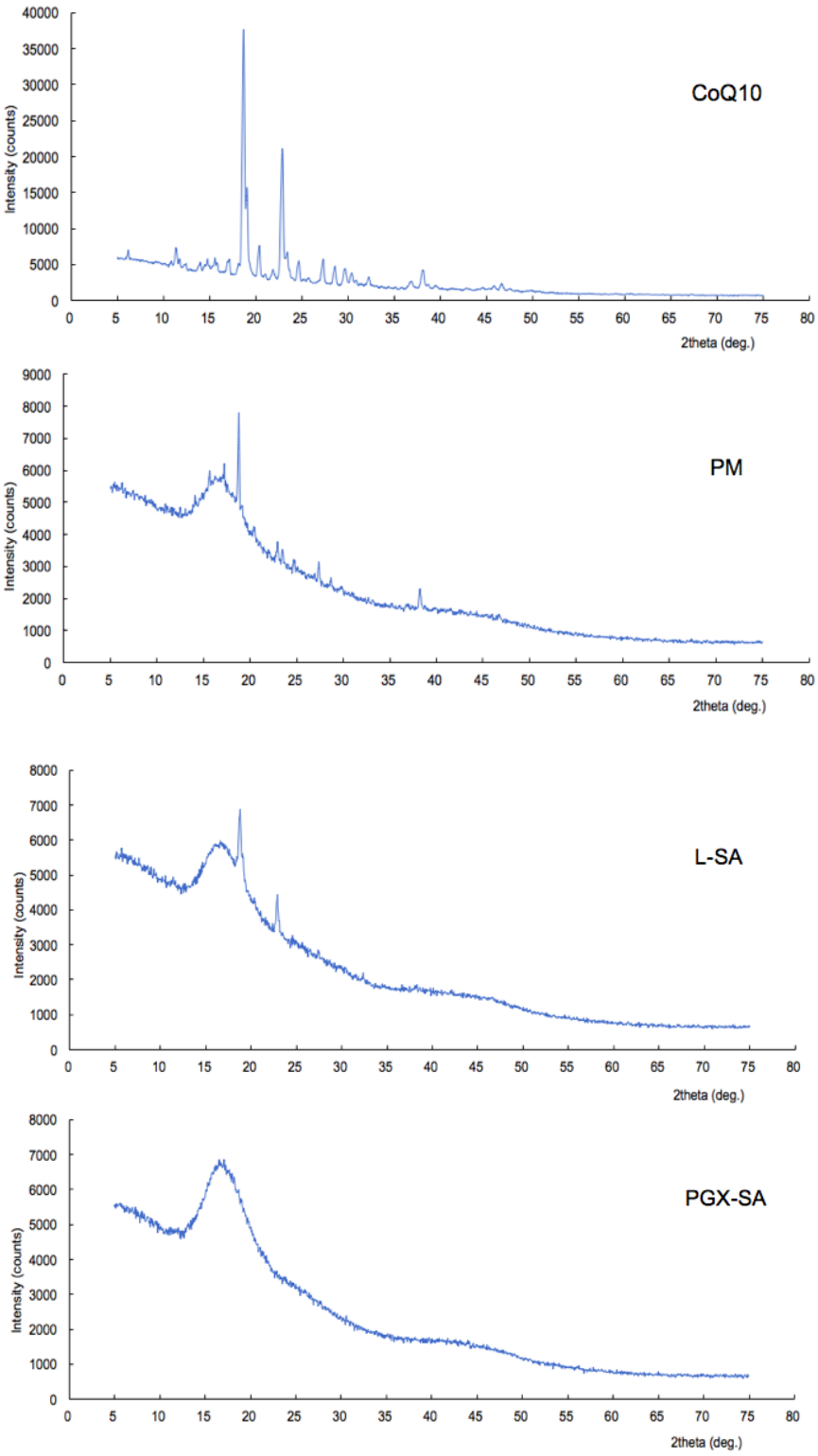

Figure 4.7 XRD spectra (from top to bottom) of CoQ10, PM, L-SA (processed at 300 bar, with 40 min & 262 mL/min, and biopolymer in original form), and PGX-SA.

4.3.6 Dispersion in aqueous system

The dispersions of PGX-SA, PM and L-SA in an aqueous system were evaluated by dispersing 10 mg of sample in 10 mL deionized water and the photographs were presented in Figure 4.8. Since the SA is a high molecular weight, long-chain polysaccharide, it forms a colloidal sol rather than a true solution and PGX-SA dispersed in water was clear. Since the CoQ10 in the PM was in crystalline aggregated form, it could not be dispersed uniformly, and it was just suspended or precipitated or formed a separate layer on top of the clear aqueous sol containing SA. On the other hand, the aqueous dispersion of the L-SA appeared cloudy compared with the PGX-SA and PM dispersions. This may be due to the particle size of the loaded CoQ10 being smaller and the hydrogen bond interactions between CoQ10 and SA within the L-SA may be leading to a structure resembling a gel. The dispersion of L-SA in water provided a more stable and uniform dispersion of CoQ10 in the aqueous system.

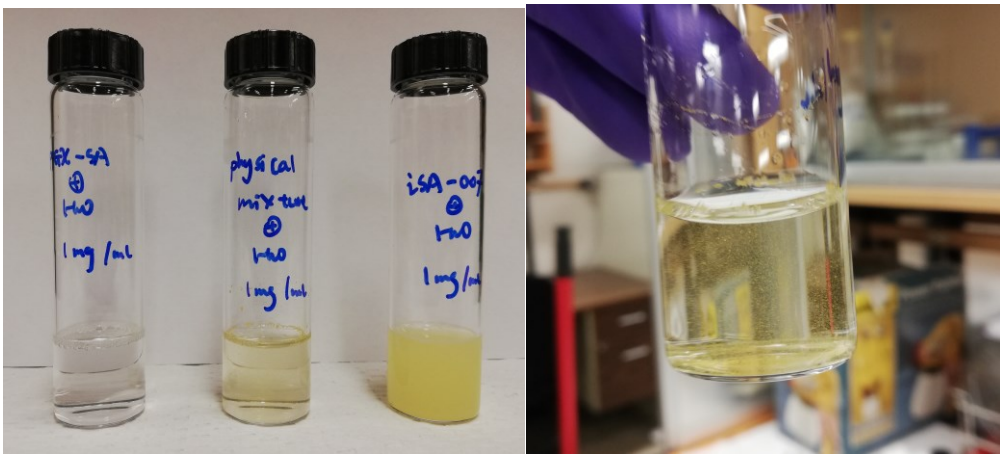

Figure 4.8 Photographs of aqueous dispersions. (left) aqueous dispersion of PGX-SA, PM, and L-SA; (right) close up of PM.

The stability of the aqueous dispersion of L-SA samples over 50 day storage in the dark environment at 4 ºC was also evaluated. As shown in Figure 4.9, a portion of the CoQ10 loaded on the SA separated and precipitated to the bottom of the sample container after 3 days, and another small portion of CoQ10 precipitated out after 50 days of storage at 4 ºC. However, a portion of the CoQ10 was still stable and uniformly dispersed in the aqueous dispersion, which maintained its yellow color even after 50 days of storage. Based on the FTIR results mentioned above for the L-SA powder, there was no new covalent bond or linkages formed after the loading process, but some interactions such as hydrogen bonding could form in the aqueous environment. Moreover, since the loading amount of CoQ10 was quite high in the L-SA, the precipitated CoQ10 might only be a small portion of the total loaded amount.

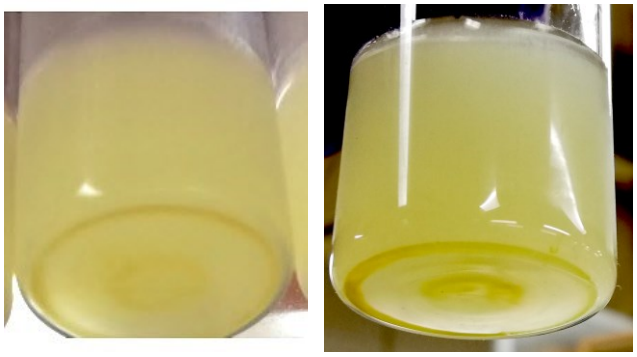

Figure 4.9 Aqueous dispersions of L-SA after 3 (left) and 50 (right) days storage at 4 ºC.

4.3.7 Zeta potential

Based on the zeta potential measurement results presented in Figure 4.10, PGX-SA, L-SA, and PM particles had an absolute value of zeta potential higher than 67 mV. It is known that particles with an absolute value of zeta potential higher than 30 mV can form stable dispersions

(dos Santos Silva et al., 2011). Therefore, all of the SA based dispersions used in this analysis were stable systems. Because the CoQ10 is a neutral molecule and the zeta potential only measures the charged molecules in the electric field, the stability of aqueous dispersions is dictated by only SA in these five dispersions, where the results are all similar, reflecting the high level of negative charge on SA. Lertsutthiwong et al. (2008) focused on encapsulation of turmeric oil by using sodium alginate. The emulsion was prepared by mixing sodium alginate aqueous solution with ethanol or acetone diluted turmeric oil, followed by crosslinking with calcium chloride, and then removal of solvent. They reported the zeta potential as -41.2 mV for this dispersion. The absolute zeta potential value obtained in this study was higher since no crosslinking was applied.

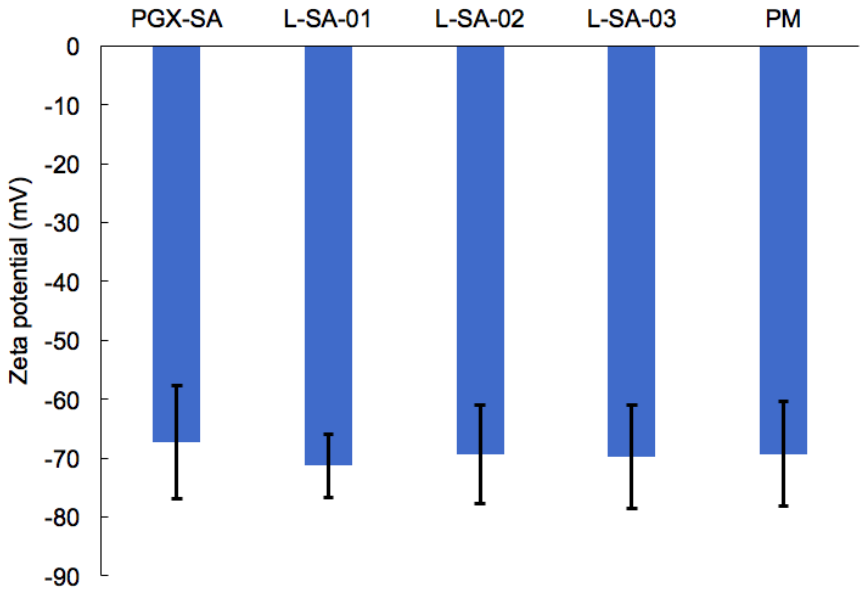

Figure 4.10 Zeta potential values of different samples (L-SA-01 was processed at 300 bar, with 40 min & 262 mL/min circulation, and biopolymer in original form; L-SA-02 was processed at similar conditions except at 200 bar; and L-SA-03 was processed at similar conditions to L-SA-01 but using biopolymer in ground form).

4.4 Conclusions

The adsorptive precipitation process is an efficient bioactive loading method for CoQ10 and PGX-SA. In this study, L-SA was prepared at different processing conditions and its physicochemical properties were determined. The CoQ10 loading content was significantly affected by the circulation time and rate. The higher the time and rate of the circulation step, the more CoQ10 was adsorbed on the surface of PGX-SA. The highest CoQ10 loading of 46.9% (w/w) was obtained at the lowest processing pressure (200 bar), which had a more efficient and faster precipitation during the depressurization step. Moreover, the ground PGX-SA (109.45 m^2/g) had a slightly higher loading than the original form (62.5 m^2/g). The CoQ10 melted and dissolved in the SC-CO_2 during the process, which resulted in the homogeneous coating on the surface of the PGX-SA. The CoQ10 loaded on the SA maintained its crystalline form. In addition, the L-SA could form a uniform aqueous dispersion, which was more uniform and stable than the dispersion of PM. The aqueous dispersion of L-SA was stable for 3 days at 4 ºC, after which some precipitate of CoQ10 was apparent, but the CoQ10 retained in the dispersion was stable for 50 days when stored in the dark environment at 4 ºC. This indicates that it would be possible to avoid precipitation by adjusting the processing parameters, and load a suitable amount of CoQ10 on the PGX-SA, which would then result in a more efficient dispersion of CoQ10 in the aqueous system. The findings demonstrate the potential of the adsorptive precipitation process for loading of CoQ10 on sodium alginate as a delivery system, targeting various aqueous-based applications.

Chapter 5: Conclusions and recommendations

5.1 Summary of key findings

The Pressurized Gas eXpanded (PGX) liquid technology is a CO_2-based novel drying method for water-soluble biopolymers, which can generate dried biopolymers with unique morphology that cannot be achieved by any other conventional drying method. Sodium alginate (SA) is a water-soluble polysaccharide extracted from brown algae, which is a long-chain, high molecular weight biopolymer utilized in many applications. However, since the PGX drying method is a relatively new technology, a few biopolymers (β-glucan, gum arabic, native corn starch granule, citrus pectin, sodium alginate, nano-composite of pectin and sodium alginate, and nanocrystalline cellulose) has been subjected to this drying technique to demonstrate its capability to handle different kinds of materials (Seifried, 2016), but only a small number of biopolymers has been tested in depth by this drying method, and there are no reports focusing on the detailed investigation of the drying of SA by the PGX technology, and its impact on sample characteristics. Therefore, the first study focused on how different processing parameters could affect the characteristics of SA (Chapter 3). After PGX processing, SA had a fibrous structure with a fine network of fibrils, rather than the fine particles with a smooth surface of the unprocessed SA. Together with the change in the morphology of the particles, the surface area increased substantially and the bulk density decreased more than 120 times compared to the unprocessed SA. Use of low concentration (1.0% w/w) of the SA aqueous solution as the feed material, low ethanol flow rate (15 g/min), with the mass flow rate ratio of 4:15:5 of aqueous

solution:ethanol:CO_2 resulted in the surface area of 164.5 m^2/g of the PGX-processed SA. Such a large increase in the surface area provided a high potential for it to be used as a carrier for bioactive compounds and improve the dispersion of hydrophobic materials in an aqueous system. Moreover, after the PGX process, DSC, FTIR, and XRD analyses indicated that more molecular interactions such as hydrogen bond formed between SA molecules and lead to a higher-ordered structure of the SA, which was also slightly more thermally stable compared to the unprocessed SA. Furthermore, the viscosity measurement indicated that the viscosity of the PGX-processed SA solution was similar to that of the unprocessed SA at the same concentration. Since viscosity is directly related to the molecular weight of the biopolymer, this was an indication that the molecular weight of the processed SA was not affected by the PGX drying process.

Based on the unique characteristic of the SA obtained from the PGX process, the second part of this thesis research was to investigate the loading of the hydrophobic CoQ10 onto the high-surface-area SA biopolymer by using the adsorptive precipitation process (Chapter 4). CoQ10 was selected for this purpose because it has many health benefits, but because of its hydrophobic and crystalline nature, its bioavailability in the human body is low, and developing aqueous-based applications is challenging. More importantly, there are no reports on the adsorptive precipitation of CoQ10 on PGX-processed SA up to now. Therefore, this study focused on how different processing parameters affect the CoQ10 loading content and the physicochemical properties of the loaded product. After determining the CoQ10 loading on PGX-SA, it was demonstrated that high circulation power (50 min X 262 mL/min), low

operation pressure (200 bar), and the biopolymer with a high surface area (ground PGX-SA) could result in higher loading of the bioactive compound. The highest loading obtained was 46.9% w/w. Also, based on the helium ion microscopy images, the adsorptive precipitation resulted in a uniform coating of CoQ10 on the surface of PGX-SA. The loaded CoQ10 maintained its crystalline form based on the results from XRD and DSC analysis. The zeta potential values of over -67 mV indicated the stability of the aqueous dispersion of the PGX-SA system. However, some of the CoQ10 precipitated to the bottom of the vial after 3 days of storage at 4 ºC. The FTIR results showed no new covalent bond formation between SA and CoQ10 after the loading process. Since the loading amount of CoQ10 in the L-SA was very high, the aqueous dispersion still maintained its light yellow color even after 50 days of storage despite having some of the CoQ10 precipitating to the bottom of the container. This indicated that there was still some CoQ10 dispersed uniformly and in a stable manner in the aqueous system, which showed potential for aqueous-based product development.

In conclusion, the PGX drying study for the SA could broaden the application of this biopolymer and provide more information for further development and modifications of the PGX technology. There is also potential for the application of the PGX drying method to the traditional SA production process. For example, the last step of the traditional SA extraction process is to precipitate the solubilized SA from the water solution (as discussed in Section 2.1.2) by applying calcium chloride or alcohol prior to drying. Instead, PGX drying technology can be directly applied to the aqueous SA solution and achieve the precipitation and drying of the

biopolymer simultaneously. Moreover, the PGX process can also contribute to the purification of SA, since the impurities would be washed away by the CO_2 + ethanol mixture. Besides, the adsorptive precipitation study findings give indications for aqueous-based applications of hydrophobic bioactives in cosmetics or food products. L-SA has potential to be used for CoQ10 delivery applications in dry-powder form, since it can uniformly hold a large amount CoQ10, and not affect the properties of the bioactive compound after the loading process. As well, the results can give suggestions for other biopolymer and bioactive compound combinations to modify and optimize the processing conditions. Moreover, the findings of this MSc research provide more information and suggestions for applying hydrophobic bioactive compounds in aqueous-based products, and developing novel bioactive delivery systems in the future. More importantly, even though the application of PGX drying process to SA was briefly mentioned previously (Seifried, 2016) to demonstrate the capabilities of the technology for the processing of different water-soluble biopolymers, detailed investigation and characterization have never been performed. Therefore, this MSc research was the first in-depth study on an ionic polysaccharide subjected to the PGX drying technology, where the properties were affected by the pH of the expanded liquid. The findings give suggestions and help better understand the capabilities and effect of PGX technology on the physicochemical properties of ionic water-soluble biopolymers.

5.2 Recommendations for future work

Based on the two studies and the key findings, future investigations are recommended as

follows:

- Investigating other mass flow rate ratios in the ternary diagram to understand better how this would affect the physicochemical properties of the PGX-processed SA.
- Lower mass flow rate ratio of the drying fluid to the SA aqueous solution (θ) can be investigated to find the optimal θ to obtain the ideal PGX-SA while minimizing the drying fluid cost.
- Other types of SA, such as those with different molecular weight and degree of polymerization could be applied to the PGX technology, to investigate if this process is capable of generating similar fibrous structures with different types of SA materials.
- The sodium content of the PGX-processed SA can be determined and compared to that of starting material in order to better understand how CO_2 dissolution in the SA sol during the PGX process affects the negatively charged groups of SA.
- Combination of SA with other compounds and materials can be applied to the PGX process to investigate if a composite with stronger affinity to the hydrophobic bioactive compound can be generated.
- The CoQ10 content of the aqueous dispersion subjected to different storage conditions can be determined as a function of time and temperature, in order to have a better understanding of the stability of the aqueous dispersion of L-SA.
- The optimal CoQ10 loading amount in the PGX-SA can be investigated, in order to obtain a more efficient aqueous-based delivery system and avoid or minimize the

CoQ10 precipitation during storage.

- The degree of crystallinity of the loaded CoQ10 in L-SA can be determined and correlated with its bioavailability.
- For the L-SA particles, the stability of the loaded CoQ10 can be investigated and compared with the unprocessed CoQ10 to determine how the biopolymer impacts its stability in powder form.
- The bioavailability and release mechanism of CoQ10 in the L-SA can be evaluated, in order to understand how these properties were affected after the loading process.

Bibliography

Alboofetileh, M., Rezaei, M., Hosseini, H., & Abdollahi, M. (2014). Antimicrobial activity of alginate/clay nanocomposite films enriched with essential oils against three common foodborne pathogens. Food Control, 36(1), 1-7.

Andresen, I. L., Skipnes, O., Smidsrød, O., Ostgaard, K., & Hemmer, P. C. (1977). Some biological functions of matrix components in benthic algae in relation to their chemistry and the composition of seawater. Cellulose Chemistry and Technology, 48(24), 361-381.

Arroyo, A., Kagan, V. E., Tyurin, V. A., Burgess, J. R., de Cabo, R., Navas, P., & Villalba, J. M. (2000). NADH and NADPH-dependent reduction of coenzyme Q at the plasma membrane. Antioxidants & Redox Signaling, 2(2), 251-262.

Bank, G., Kagan, D., & Madhavi, D. (2011). Coenzyme Q10: clinical update and bioavailability. Journal of Evidence-Based Complementary & Alternative Medicine, 16(2), 129-137.

Barakat, A., Shegokar, R., Dittgen, M., & Müller, R. H. (2013). Coenzyme Q10 oral bioavailability: effect of formulation type. Journal of Pharmaceutical Investigation, 43(6), 431-451.

Battino, M., Ferreiro, M. S., Bompadre, S., Leone, L., Mosca, F., & Bullon, P. (2001). Elevated hydroperoxide levels and antioxidant patterns in papillon-lefèvre syndrome. Journal of Periodontology, 72(12), 1760-1766.

Bhandari, K. H., Newa, M., Kim, J. A., Yoo, B. K., Woo, J. S., Lyoo, W. S., ... & Yong, C. S. (2007). Preparation, characterization and evaluation of coenzyme Q10 binary solid dispersions for enhanced solubility and dissolution. Biological and Pharmaceutical Bulletin, 30(6), 1171-1176.

Bhardwaj, T. R., Kanwar, M., Lal, R., & Gupta, A. (2000). Natural gums and modified natural gums as sustained-release carriers. Drug Development and Industrial Pharmacy, 26(10), 1025-1038.

Bhattarai, N., Li, Z., Edmondson, D., & Zhang, M. (2006). Alginate-based nanofibrous scaffolds: structural, mechanical, and biological properties. Advanced Materials, 18(11), 1463-1467.

Bierhalz, A. C. K., da Silva, M. A., & Kieckbusch, T. G. (2012). Natamycin release from alginate/pectin films for food packaging applications. Journal of Food Engineering, 110(1), 18-25.

Bouchard, A., Jovanović, N., Hofland, G. W., Jiskoot, W., Mendes, E., Crommelin, D. J., & Witkamp, G. J. (2008). Supercritical fluid drying of carbohydrates: selection of suitable excipients and process conditions. European Journal of Pharmaceutics and Biopharmaceutics, 68(3), 781-794.

Brandt, U. (1999). Proton translocation in the respiratory chain involving ubiquinone–a hypothetical semiquinone switch mechanism for complex I. Biofactors, 9(2-4), 95-101.

Brunner, G. (2005). Supercritical fluids: technology and application to food processing. Journal of Food Engineering, 67(1-2), 21-33.

Chen, S., Liu, W., Wan, J., Cheng, X., Gu, C., Zhou, H., ... & Yang, X. (2013). Preparation of Coenzyme Q10 nanostructured lipid carriers for epidermal targeting with high-pressure microfluidics technique. Drug Development and Industrial Pharmacy, 39(1), 20-28.

Cheuk, S. Y., Shih, F. F., Champagne, E. T., Daigle, K. W., Patindol, J. A., Mattison, C. P., & Boue, S. M. (2015). Nano-encapsulation of coenzyme Q10 using octenyl succinic anhydride modified starch. Food Chemistry, 174, 585-590.

Chiu, H. Y., Lee, M. J., & Lin, H. M. (2008). Vapor− liquid phase boundaries of binary mixtures of carbon dioxide with ethanol and acetone. Journal of Chemical & Engineering Data, 53(10), 2393-2402.

Comin, L. M., Temelli, F., & Saldaña, M. D. (2012). Barley β-glucan aerogels via supercritical CO_2 drying. Food Research International, 48(2), 442-448.

Couto, R., Seifried, B., Moquin, P., & Temelli, F. (2018a). Coenzyme Q10 solubility in supercritical CO_2 using a dynamic system. Journal of CO_2 Utilization, 24, 315-320.

Couto, R., Seifried, B., Yépez, B., Moquin, P., & Temelli, F. (2018b). Adsorptive precipitation of co-enzyme Q10 on PGX-processed β-glucan powder. The Journal of Supercritical Fluids, 141, 157-165.

Couvreur, P., & Vauthier, C. (1991). Polyalkylcyanoacrylate nanoparticles as drug carrier: present state and perspectives. Journal of Controlled Release, 17(2), 187-198.

Crane, F. L. (2001). Biochemical functions of coenzyme Q10. Journal of the American College of Nutrition, 20(6), 591-598.

Debenedetti, P. G., Tom, J. W., Kwauk, X., & Yeo, S. D. (1993). Rapid expansion of supercritical solutions (RESS): fundamentals and applications. Fluid Phase Equilibria, 82, 311-321.

Donnan, F. G., & Rose, R. C. (1950). Osmotic pressure, molecular weight, and viscosity of sodium alginate. Canadian Journal of Research, 28(3), 105-113.

dos Santos Silva, M., Cocenza, D. S., Grillo, R., de Melo, N. F. S., Tonello, P. S., de Oliveira, L. C., ... & Fraceto, L. F. (2011). Paraquat-loaded alginate/chitosan nanoparticles: preparation, characterization and soil sorption studies. Journal of Hazardous Materials, 190(1-3), 366-374.

Draget, K. I. (2009). Alginates. In “Handbook of Hydrocolloids” (pp. 807-828). Woodhead Publishing. Cambridge, U.K.

Durling, N. E., Catchpole, O. J., Tallon, S. J., & Grey, J. B. (2007). Measurement and modelling of the ternary phase equilibria for high pressure carbon dioxide–ethanol–water mixtures. Fluid Phase Equilibria, 252(1-2), 103-113.

Espuelas, M. S., Legrand, P., Irache, J. M., Gamazo, C., Orecchioni, A. M., Devissaguet, J. P., & Ygartua, P. (1997). Poly (ε-caprolacton) nanospheres as an alternative way to reduce amphotericin B toxicity. International Journal of Pharmaceutics, 158(1), 19-27.

Gacesa, P., Caswell, R. C., & Kille, P. (1989). Bacterial alginases. In “Pseudomonas aeruginosa Infection” (Vol. 42, pp. 67-71). Karger Publishers. Copenhagen, Denmark.

Gao, X., Nishimura, K., Hirayama, F., Arima, H., Uekama, K., Schmid, G., ... & Fukumi, H. (2006). Enhanced dissolution and oral bioavailability of coenzyme Q10 in dogs obtained by inclusion complexation with γ-cyclodextrin. Asian Journal of Pharmaceutical Sciences, 1(2), 95-102.

García-González, C. A., & Smirnova, I. (2013). Use of supercritical fluid technology for the production of tailor-made aerogel particles for delivery systems. The Journal of Supercritical Fluids, 79, 152-158.

Gombotz, W. R., & Wee, S. (1998). Protein release from alginate matrices. Advanced Drug Delivery Reviews, 31(3), 267-285.

Gorle, B. S. K., Smirnova, I., & Arlt, W. (2010). Adsorptive crystallization of benzoic acid in aerogels from supercritical solutions. The Journal of Supercritical Fluids, 52(3), 249-257.

Grasdalen, H. (1983). High-field, ^{1}H-NMR spectroscopy of alginate: sequential structure and linkage conformations. Carbohydrate Research, 118, 255-260.

Grasdalen, H., Larsen, B., Smidsréd, O. (1977). ^{13}C-NMR studies of alginate. Carbohydrate Research, 56, 11-15.

Gurikov, P., & Smirnova, I. (2018). Amorphization of drugs by adsorptive precipitation from supercritical solutions: A review. The Journal of Supercritical Fluids, 132, 105-125.

Ha, S. J., Kim, S. Y., Seo, J. H., Oh, D. K., & Lee, J. K. (2007). Optimization of culture conditions and scale-up to pilot and plant scales for coenzyme Q 10 production by Agrobacterium tumefaciens. Applied Microbiology and Biotechnology, 74(5), 974-980.

Haug, A. (1964). Composition and properties of alginates. Thesis. Norwegian Institute of Technology, Trondheim, Norway.

Haug, A., & Larsen, B. (1963). The solubility of alginate at low pH. Acta Chemica Scandinavica, 17(6), 1653-62.

Haug, A., Myklestad, S., Larsen, B., & Smidsrød, O. (1967). Correlation between chemical

structure and physical properties of alginates. Acta Chemica Scandinavica, 21(3), 768-78.

Health Canada. (2007). Coenzyme Q10 (Ubiquinone-10). Ottawa, ON: Health Canada. http://webprod.hc-sc.gc.ca/nhpid-bdipsn/atReq.do?atid=coenzyme.q10&lang=eng (accessed on May 29th, 2019)

Hertz, N., & Lister, R. E. (2009). Improved survival in patients with end-stage cancer treated with coenzyme Q10 and other antioxidants: a pilot study. Journal of International Medical Research, 37(6), 1961-1971.

Hoppe, U., Bergemann, J., Diembeck, W., Ennen, J., Gohla, S., Harris, I., ... & Schachtschabel, D. (1999). Coenzyme Q10, a cutaneous antioxidant and energizer. Biofactors, 9(2-4), 371-378.

Hsu, C. H., Cui, Z., Mumper, R. J., & Jay, M. (2003). Preparation and characterization of novel coenzyme Q 10 nanoparticles engineered from microemulsion precursors. AAPS Pharmaceutical Science and Technology, 4(3), 24-35.

Jeya, M., Moon, H. J., Lee, J. L., Kim, I. W., & Lee, J. K. (2010). Current state of coenzyme Q 10 production and its applications. Applied Microbiology and Biotechnology, 85(6), 1653-1663.

Joseph, I., & Venkataram, S. (1995). Indomethacin sustained release from alginate-gelatin or pectin-gelatin coacervates. International Journal of Pharmaceutics, 126(1-2), 161-168.

Kim, E. A., Kim, J. Y., Chung, H. J., & Lim, S. T. (2012). Preparation of aqueous dispersions of coenzyme Q10 nanoparticles with amylomaize starch and its dextrin. LWT-Food Science and Technology, 47(2), 493-499.

Kjellow, A. W., Henriksen, O., Sørensen, J. C., Johannsen, M., & Felby, C. (2010). Partitioning of organic biocides between wood and supercritical carbon dioxide. The Journal of Supercritical Fluids, 52(1), 1-5.

Kommuru, T. R., Gurley, B., Khan, M. A., & Reddy, I. K. (2001). Self-emulsifying drug delivery systems (SEDDS) of coenzyme Q10: formulation development and bioavailability

assessment. International Journal of Pharmaceutics, 212(2), 233-246.

Kong, L., Yu, L., Feng, T., Yin, X., Liu, T., & Dong, L. (2015). Physicochemical characterization of the polysaccharide from *Bletilla striata*: Effect of drying method. Carbohydrate Polymers, 125, 1-8.

Kwon, S. S., Nam, Y. S., Lee, J. S., Ku, B. S., Han, S. H., Lee, J. Y., & Chang, I. S. (2002). Preparation and characterization of coenzyme Q10-loaded PMMA nanoparticles by a new emulsification process based on microfluidization. Colloids and Surfaces A: Physicochemical and Engineering Aspects, 210(1), 95-104.

Larsen, B., Smidsrød, O., Painter, T. J., & Haug, A. R. N. E. (1970). Calculation of the nearest-neighbour frequencies in fragments of alginate from the yields of free monomers after partial hydrolysis. Acta Chemica Scandinavica, 24(2), 726-728.

Lawrie, G., Keen, I., Drew, B., Chandler-Temple, A., Rintoul, L., Fredericks, P., & Grøndahl, L. (2007). Interactions between alginate and chitosan biopolymers characterized using FTIR and XPS. Biomacromolecules, 8(8), 2533-2541.

Lee, K. Y., & Mooney, D. J. (2012). Alginate: properties and biomedical applications. Progress in Polymer Science, 37(1), 106-126.

Lenaz, G., Fato, R., Di Bernardo, S., Jarreta, D., Costa, A., Genova, M. L., & Castelli, G. P. (1999). Localization and mobility of coenzyme Q in lipid bilayers and membranes. Biofactors, 9(2-4), 87-93.

Leo, W. J., McLoughlin, A. J., & Malone, D. M. (1990). Effects of sterilization treatments on some properties of alginate solutions and gels. Biotechnology Progress, 6(1), 51-53.

Lertsutthiwong, P., Noomun, K., Jongaroonngamsang, N., Rojsitthisak, P., & Nimmannit, U. (2008). Preparation of alginate nanocapsules containing turmeric oil. Carbohydrate Polymers, 74(2), 209-214.

Lester, R. L., & Crane, F. L. (1959). The natural occurrence of coenzyme Q and related compounds. Journal of Biological Chemistry, 234(8), 2169-2175.

Liu, N., Couto, R., Seifried, B., Moquin, P., Delgado, L., & Temelli, F. (2018). Characterization of oat β-glucan and coenzyme Q10-loaded β-glucan powders generated by the pressurized gas-expanded liquid (PGX) technology. Food Research International, 106, 354-362.

Martín, Á., Pham, H. M., Kilzer, A., Kareth, S., & Weidner, E. (2010). Micronization of polyethylene glycol by PGSS (Particles from Gas Saturated Solutions)-drying of aqueous solutions. Chemical Engineering and Processing: Process Intensification, 49(12), 1259-1266.

Matias, A. A., Nunes, A. V., Casimiro, T., & Duarte, C. M. (2004). Solubility of coenzyme Q10 in supercritical carbon dioxide. The Journal of Supercritical Fluids, 28(2-3), 201-206.

Nep, E. I., & Conway, B. R. (2011). Physicochemical characterization of grewia polysaccharide gum: Effect of drying method. Carbohydrate Polymers, 84(1), 446-453.

Nicolson, G. L., & Conklin, K. A. (2008). Reversing mitochondrial dysfunction, fatigue and the adverse effects of chemotherapy of metastatic disease by molecular replacement therapy. Clinical & Experimental Metastasis, 25(2), 161-169.

Onsøyen, E. (1997). Alginates. In “Thickening and Gelling Agents for Food” (pp. 22-44). Springer, Boston, MA.

Painter, T. J., Smidsrød, O., & Haug, A. (1968). A computer study of the changes in composition-distribution occurring during random depolymerisation of a binary linear heteropolysaccharide. Acta Chemica Scandinavica, 22(5), 1637-1648.

Palamakula, A., Soliman, M., & Khan, M. M. A. (2005). Regional permeability of coenzyme Q10 in isolated rat gastrointestinal tracts. Die Pharmazie-An International Journal of Pharmaceutical Sciences, 60(3), 212-214.

Park, S. J., & Yeo, S. D. (2008). Recrystallization of caffeine using gas antisolvent process. The Journal of Supercritical Fluids, 47(1), 85-92.

Patil, R. T., & Speaker, T. J. (1997). Retention of trypsin activity in spermine alginate microcapsules. Journal of Microencapsulation, 14(4), 469-474.

Pranoto, Y., Salokhe, V. M., & Rakshit, S. K. (2005). Physical and antibacte rial properties of alginate-based edible film incorporated with garlic oil. Food Research International, 38(3), 267-272.

Prosapio, V., Reverchon, E., & De Marco, I. (2014). Antisolvent micronization of BSA using supercritical mixtures carbon dioxide+ organic solvent. The Journal of Supercritical Fluids, 94, 189-197.

R Core Team (2015). R: A language and environment for statistical computing. R Foundation for Statistical Computing, Vienna, Austriahttps://www.R-project.org/, Accessed on: August 21st, 2019.

Regand, A., & Goff, H. D. (2003). Structure and ice recrystallization in frozen stabilized ice cream model systems. Food Hydrocolloids, 17(1), 95-102.

Rhim, J. W. (2004). Physical and mechanical properties of water resistant sodium alginate films. LWT-Food Science and Technology, 37(3), 323-330.

Saini, R. (2011). Coenzyme Q10: the essential nutrient. Journal of Pharmacy and Bioallied Sciences, 3(3), 466-467.

Sarmento, B., Ferreira, D., Veiga, F., & Ribeiro, A. (2006). Characterization of insulin-loaded alginate nanoparticles produced by ionotropic pre-gelation through DSC and FTIR studies. Carbohydrate Polymers, 66(1), 1-7.

Sartori, C., Finch, D. S., Ralph, B., & Gilding, K. (1997). Determination of the cation content of alginate thin films by FTIR spectroscopy. Polymer, 38(1), 43-51.

Seifried, B. (2010). Physicochemical properties and microencapsulation process development for fish oil using supercritical carbon dioxide. PhD thesis. University of Alberta, Edmonton, Canada.

Seifried, B. (2016). PGX technology: an enabling technology for generating biopolymer fibrils, particles, aerogels and nano-composites. Proceedings of the 15th European Meeting on Supercritical Fluids, Essen, Germany, May 8-11, 2016.

Sime, W. J. (1990). Alginates. In “Food Gels,” ed. Harris, P. Elsevier Applied Food Science Series. Springer, Dordrecht.

Skjak-Braek, G., Smidsrød, O., & Larsen, B. (1986). Tailoring of alginates by enzymatic modification in vitro. International Journal of Biological Macromolecules, 8(6), 330-336.

Smidsréd, O. (1973). Some physical properties of alginates in solution and in the gel state. Thesis. Norwegian Institute of Technology, Trondheim, Norway.

Smidsrød, O. (1974). Molecular basis for some physical properties of alginates in the gel state. Faraday Discussions of the Chemical Society, 57, 263-274.

Song, Y., & Buettner, G. R. (2010). Thermodynamic and kinetic considerations for the reaction of semiquinone radicals to form superoxide and hydrogen peroxide. Free Radical Biology and Medicine, 49(6), 919-962.

Stuart, B. (2004). “Infrared Spectroscopy: Fundamentals and Applications”. J. Wiley. Chichester, West Sussex, England.

Sun-Waterhouse, D., Wadhwa, S. S., & Waterhouse, G. I. (2013). Spray-drying microencapsulation of polyphenol bioactives: a comparative study using different natural fibre polymers as encapsulants. Food and Bioprocess Technology, 6(9), 2376-2388.

Takahashi, T., Okamoto, T., Mori, K., Sayo, H., & Kishi, T. (1993). Distribution of ubiquinone and ubiquinol homologues in rat tissues and subcellular fractions. Lipids, 28(9), 803-809.

Takeuchi, H., Yasuji, T., Hino, T., Yamamoto, H., & Kawashima, Y. (1998). Spray-dried composite particles of lactose and sodium alginate for direct tabletting and controlled releasing. International journal of pharmaceutics, 174(1-2), 91-100.

Tan, L. H., Chan, L. W., & Heng, P. W. S. (2009). Alginate/starch composites as wall material to achieve microencapsulation with high oil loading. Journal of Microencapsulation, 26(3), 263-271.

Temelli, F., & Seifried, B. (2016). Supercritical fluid treatment of high molecular weight

biopolymers. U.S. Patent No. 9,249,266. Washington, DC: U.S. Patent and Trademark Office.

Toews, K. L., Shroll, R. M., Wai, C. M., & Smart, N. G. (1995). pH-defining equilibrium between water and supercritical CO_2. Influence on SFE of organics and metal chelates. Analytical Chemistry, 67(22), 4040-4043.

Toft, K., Grasdalen, H., & Smidsrod, O. (1986). Synergistic gelation of alginates and pectins. In ACS Symposium Series (Vol. 310, pp. 117-132).

Tønnesen, H. H., & Karlsen, J. (2002). Alginate in drug delivery systems. Drug Development and Industrial Pharmacy, 28(6), 621-630.

Vendruscolo, C. W., Ferrero, C., Pineda, E. A. G., Silveira, J. L. M., Freitas, R. A., Jimenez-Castellanos, M. R., et al. (2009). Physicochemical and mechanical characterization of galactomannan from Mimosa scabrella: Effect of drying method. Carbohydrate Polymers, 76, 86–93.

Wyman, M., Leonard, M., & Morledge, T. (2010). Coenzyme Q10: a therapy for hypertension and statin-induced myalgia? Cleveland Clinic Journal of Medicine, 77(7), 435-442.

Yamamoto, Y., & Yamashita, S. (1997). Plasma ratio of ubiquinol and ubiquinone as a marker of oxidative stress. Molecular Aspects of Medicine, 18, 79-84.

Yeo, S. D., & Kiran, E. (2005). Formation of polymer particles with supercritical fluids: a review. The Journal of Supercritical Fluids, 34(3), 287-308.

Yeo, S. D., Debenedetti, P. G., Radosz, M., & Schmidt, H. W. (1993). Supercritical antisolvent process for substituted para-linked aromatic polyamides: phase equilibrium and morphology study. Macromolecules, 26(23), 6207-6210.

York, P. (1983). Solid-state properties of powders in the formulation and processing of solid dosage forms. International Journal of Pharmacy, 14, 1–28.

Yu, L. (2001). Amorphous pharmaceutical solids: preparation, characterization and stabilization.

Advanced drug delivery reviews, 48(1), 27-42.